Accepted Basin Research, 02/2/21

The formation of the Sichuan Basin, South China, during the Late Ediacaran to Early Cambrian

Zhidong Gu[1,2], Lidia Lonergan[2], Xiufen Zhai[1], Baomin Zhang[1], Weihua Lu[1]

1. Research Institute of Petroleum Exploration and Development (RIPED), PetroChina, Beijing, China
2. Department of Earth Science and Engineering, Imperial College London, London, UK

Abstract

The Upper Ediacaran to Lower Cambrian of the Sichuan Basin in South China has long been considered to be dominated by shallow-water deposition. Hydrocarbon exploration, however, has revealed that a NW-SE trending intraplatform trough formed in the basin during the same period. Although different models have been proposed, the formation and evolution of the trough are still not fully understood. In this study, we investigate both the origin of the intraplatform trough and the formation of the Sichuan Basin by integrating seismic interpretation, well correlation, and tectonic subsidence analysis. The seismic and well data clearly show three stages of development of the trough. The first stage, in the early Late Ediacaran, is characterized by considerable thinning of the lower two members of the Upper Ediacaran from the platform margins to the trough. In the second stage, in the late Late Ediacaran, the platform margins backstepped and the extent of the trough expanded significantly to a width of ~400 km. The third stage, in the early Early Cambrian, was dominated by gradual filling of the trough and onlapping of the platform margins. Backstripped tectonic subsidence curves show one, or two closely spaced episodes of linear subsidence starting at ~550 Ma and then decreasing exponentially until ~450 Ma. The shape of the subsidence curves is consistent with formation of the Sichuan Basin by low, and slow amounts of lithospheric stretching of thickened cratonic lithosphere. The tectonic subsidence increases from the centre to the NW of the basin. Interestingly the margins of the trough do not correlate with contoured values of increased tectonic subsidence and we infer that the trough was a palaeogeographic embayment in a large carbonate platform that developed in a broad, ramp-like area of slow and low subsidence tilting down to the proto-Tethyan ocean located to the NW of the basin.

KEYWORDS
Sichuan Basin, South China, Late Ediacaran, Early Cambrian, intraplatform trough, basin formation, tectonic subsidence

1 INTRODUCTION

The Sichuan Basin located on the northwest South China craton in central China is a long-lived basin with a very thick sedimentary infill (>10 km) that extends from Neoproterozoic (Ediacaran) to

Quaternary in age (Figure 1). Today it is surrounded by mountain belts on all sides, and it has had a multiphase history. Its early fill, from Ediacaran to Middle Triassic times is dominated by mainly shallow marine carbonate deposition (e.g. Cao et al., 1979; Zhang et al., 1979; Huang, 1985; Korsch, Mai, Sun, & Gorter, 1991; Guo et al., 1996). Thereafter it developed as a foreland basin to orogenic belts forming to the west, north and east, and was infilled by terrestrial sediments (Figures 1b, c; Chen, Wilson, Luo, & Deng, 1994; Meng, Zhang, Yu, & Mei, 1996; Yong, Allen, Densmore, & Qiang, 2003). However, the late Neoproterozoic to early Palaeozoic development of the Sichuan Basin remains poorly understood. Mechanisms such as formation on a platform margin adjacent to an ocean (Bally et al., 1986); a rift evolving to a passive margin (Wang & Li, 2003) or formation as an intracratonic basin (Korsch, Mai, Sun, & Gorter, 1991) have all been proposed. In this paper we aim to investigate the mechanisms by which the Sichuan Basin formed in Ediacaran to Cambrian times, by integrating the analysis of new seismic reflection and well datasets with tectonic subsidence modelling.

It is generally accepted that passive margins form by lithospheric extension followed by thermal cooling, whereby an original continental rift, with continued lithospheric stretching evolves into an oceanic basin (e.g. McKenzie, 1978; Watts & Steckler, 1979; Le Pichon & Sibuet, 1981; Stecker & Watts, 1981; Beaumont, Keen, & Boutilier, 1982). Consequently, the passive margin generally records the history of continental rifting, and the subsequent thermal subsidence on the continental margin. Passive margins are underlain by older rift systems, with normal-fault associated syn-rift sedimentary sequences that are normally continental in origin. During the thermal cooling phase, in what is often referred to as the 'drift' phase, seaward thickening prisms of marine sedimentary rocks are deposited on the passive margin (Steckler & Watts, 1981). The syn-rift phase is often separated from the drift phase by a 'break-up' unconformity.

Cratonic basins are an associated, but less well understood basin type, with regional tectonic subsidence curves that show initially fast subsidence which then decreases in rate indicative of thermal cooling (Nunn & Sleep, 1984; Xie & Heller, 2009), however they tend to lack evidence of normal faulting typical of lithospheric extension. These basins are generally located on stable thick cratons, are very long lived (100s of millions of years) and have near layer-cake stratigraphy (Sloss, 1963; Sloss & Speed, 1974; Quinlan, 1987). Examples include the Michigan, Williston and Illinois Basins in North America; West Siberian Basin, Congo Basin in Africa and the Parnaíba Basin in Brazil (Bond & Kominz, 1984; Hartley & Allen, 1994; Tozer, Watts, & Daly, 2017; Vyssotski, Vyssotski, & Nezhdanov, 2006; Watts, Tozer, Daly & Smith, 2018). Although the majority of intracratonic basins are located away from plate margins there are some which are connected by a rift or failed rift zone to the ocean, as in the Lower Palaeozoic Illinois Basin of USA (Braile, Hinze, Keller, Lidiak, & Sexton, 1986) and the West Siberian Basin (Vyssotski, Vyssotski, & Nezhdanov, 2006).

Armitage and Allen (2010) and Allen and Armitage (2012) suggest that cratonic basins can be explained by very low values of stretching with low strain rate extension accompanied and followed by cooling of the underlying lithosphere generating subsidence. However, many other geodynamic mechanisms have also been proposed to play some role, including dynamic topography originating from large-scale mantle flow (Liu, 1979; Hartley & Allen, 1994; Burgess, Gurnis, & Moresi, 1997; Farrington, Stegman, Moresi, Sandiford, & May, 2010); small-scale convection or draining of ponded plume material (Sleep, 2009; 2018); densification of underlying mantle imposing a subcrustal load (e.g. Fowler & Nisbet, 1985; Downey & Gurnis, 2009) and rapid removal of thickened crust by erosion over tens of Myrs where thickening increases the temperature of the lithosphere. The subsequent rapid erosion causes cooling and subsidence (McKenzie & Priestley, 2016; McKenzie & Rodríguez Tribaldos, 2018).

The late Ediacaran to Middle Triassic infill, with a cumulative thickness of 6000-7000 m (Zhu, Wang, Xie, Xie, & Liu, 2015) of the Sichuan Basin consists of several sedimentary mega-sequences separated by regional unconformities, dominated by shallow marine to marginal marine carbonate palaeoenvironments, but curiously with no evidence of any major extensional faults that might indicate formation by lithospheric extension. In this sense there are elements of the Late Neoproterozoic to Palaeozoic history of the Sichuan Basin that might suggest that it formed as a cratonic basin. Korsch et al. (1991) interpreted the basin as a large intracratonic basin that started to form in the Late Proterozoic (Sinian). They present tectonic subsidence curves that indicate that in its early phases the basin formed as a complicated extensional basin. Bally et al. (1986) who mainly concentrated on the Late Palaeozoic and Mesozoic history of the basin, recognised that the Upper Ediacaran to Permian history was dominated by platform sequences, potentially on a passive margin, and Wang and Li (2003) relate the formation of the Sichuan Basin to the wider break-up of the Neoproterozoic Rodinia supercontinent. They identify two rift basins (Kangdian and Nanhua) that formed before ~750 Ma from outcrops in areas currently to the southwest and east of the Sichuan Basin. They propose that rifting ended by ~690 Ma and that the late Ediacaran-Cambrian platform carbonate areas of the Sichuan Basin formed a sag phase to the earlier rifting events.

The post-Permian evolution of the Sichuan Basin is well documented where seismic data, thickness maps, and subsidence modelling show that since the late Triassic, the Sichuan Basin has been a foreland basin where the subsidence can be attributed to the flexural loading of mountain belts forming on the west (Longmenshan-Indosinian orogeny and closure of Songpan-Ganzi ocean; Burchfiel, Chen, Liu, & Royden, 1995; Richardson et al., 2008; Yan et al., 2018), north (Dabashan and Micangshan part of the Central China orogenic belt formed due to the collision of North and South China cratons; Dong et al., 2015) and east (East Sichuan-Xuefengshan fold belt) sides of the basin (Yong, Allen, Densmore, & Qiang, 2003; Wang, Zhang, Fan, & Peng, 2005; Gu et al., 2020).

A present-day simplified regional cross-section, oriented SE to NW across the basin from the east Sichuan fold and thrust belt to the Longmenshan (Figure 1c) shows a 'classic' foreland basin geometry within the upper Triassic to Quaternary where the clastic sedimentary infill thickens into the Longmenshan fold and thrust belt.

The formation mechanism of the early Sichuan Basin remains enigmatic, but due to the intense hydrocarbon exploration of the last two decades (e.g. Zou et al., 2014; Zhu, Wang, Xie, Xie, & Liu, 2015; Fu et al., 2020) targeting the Ediacaran and Cambrian there are now extensive new datasets that allow us to address this problem. Here we integrate a large seismic and well dataset (including core and well logs), from the centre and west of the basin with tectonic subsidence analyses to present a new interpretation of the formation of the Sichuan Basin in the late Neoproterozoic (Ediacaran) to Cambrian.

Recent work based on oil company data (e.g. Zou et al., 2014; Liu et al., 2015; Gu et al., 2016; Liu et al., 2017; Zhou et al., 2017) has further revealed that though, in general, the late Ediacaran to early Cambrian succession is dominated by platform and lagoon carbonates in the Sichuan Basin, there is a broadly linear area ～100 km wide widening to the NW- that trends NW-SE, in the west-central part of the basin, where deeper water facies have been drilled, and very clear platform margins with microbial build ups can be observed on seismic data surrounding this 'trough' (Figure 2). The facies are confirmed from numerous well penetrations (Zou et al., 2014; Gu et al., 2016; Zhou et al., 2017). We refer to this feature as an 'intraplatform trough' in this paper, in a descriptive sense with no genetic implication.

Several hypotheses have been proposed to explain the existence of such a trough in an area dominated by shallow water carbonate deposition. These fall broadly into two types -one set of authors have proposed that the trough is an erosional feature where there was localised uplift in the area (due to Ediacaran Tongwan tectonic events), followed by erosion that removed the upper part of the Ediacaran in the trough and subsequent subsidence (Wang et al., 2014; Liu et al., 2017; Zhou et al., 2017). This model requires that the crust first uplifts along a narrow belt with a width of ～50-200 km at the end of the Late Ediacaran, and then quickly subsides in the same area during the earliest Cambrian. Uplift might be expected to tilt strata, and any subsequent erosion would form angular unconformities, yet there are no angular unconformities visible in the seismic data across the trough. A second group of authors propose that the trough is a small rift basin formed due to lithospheric extension (Gu & Wang, 2014; Liu, Ning, & Xie, 2015; Wei et al., 2015; Du et al., 2016). However, there is no evidence on seismic data for any significant extensional faults, with growth strata. So not only is the formation of the Ediacaran to Cambrian Sichuan Basin poorly understood it also contains an enigmatic 'trough' with deeper water facies which has hitherto proved difficult to explain.

The aim of this paper is to shed light on the formation mechanisms of both the Sichuan Basin and the trough based on an integrated analysis of seismic data, well correlation, and tectonic subsidence. More than 1,000 2-D seismic reflection lines and 10,000 km^2 of 3-D seismic reflection data from the western and central Sichuan Basin have been used to map the trough. Over 100 wells, with core and wireline logs have been used to reconstruct the sedimentary facies and palaeogeography for key stratigraphic intervals within the upper Ediacaran in the trough and surrounding areas of the basins.

2 GEOLOGICAL SETTING

2.1 Geological history of the South China craton

The Lower Neoproterozoic to Lower Paleozoic records a significant reorganization of the continental blocks that formed the Rodinia supercontinent at ~900 Ma to their dispersal and reassembly into the Gondwana supercontinent by 450-500 Ma (Cocks & Torsvik, 2013; Torsvik & Cocks, 2017; Cawood et al., 2018). The South China craton consists of the Yangtze and Cathaysian blocks that were assembled during the Jiangnan orogeny between ca. 980-810 Ma, as part of Rodinia (Zhao & Cawood, 2012; Charvet, 2013; Cawood et al., 2018; Chen et al., 2018; Zhao, Li, Liu, & Wang, 2018). Palaeomagnetic data, the study of sedimentary successions and provenance analyses, show that during the break-up of Rodinia the South China craton moved southward from a northern polar latitude to low-latitudes during the Late Tonian to Cryogenian, (~850 - 635 Ma) arriving at an equatorial position during the Ediacaran to Early Cambrian, although its position within the Rodinia supercontinent is much debated (Zhang et al., 2013, 2015; Cawood, Wang, Xu, & Zhao, 2013; Merdith et al., 2017; Torsvik & Cocks, 2017; Cawood et al., 2018; Wang et al., 2021). Part of this debate concerns the origin of Neoproterozoic magmatic rocks on the western margin of the Sichuan Basin (known as the Panxi-Hannan magmatic belt). They have been attributed to either a volcanic arc in a subduction setting between ca. 960-720 Ma (Chen, Sun, Long, Zhao, & Yuan, 2016; Chen et al., 2018; Li, Wang, & Gu, 2018; Zhao, Li, Liu, & Wang, 2018), or to an intracontinental rift setting related to mantle plume activity (Li et al., 1999, 2003, 2008; Zhao & Cawood, 2012). Despite the disagreements around the position of South China in Rodinia the majority of recent plate reconstructions suggest that major oceans that had formed during, and after, the break-up of Rodinia lay to the north and west of the Sichuan Basin (Xu et al., 2013; Zhang et al., 2015; Torsvik & Cocks, 2017; Cawood et al., 2018). Accordingly, by the Ediacaran and continuing into the Cambrian, the western margin of the Sichuan Basin, within the South China craton lay adjacent to the Proto-Tethys ocean, and would appear therefore to have been located in a passive margin setting.

2.2 Ediacaran and Cambrian Stratigraphy

The earliest sedimentary cover above seismic acoustic basement in the west and central Sichuan Basin (Figures 1, 3) is the Ediacaran System as revealed by wells within the basin and outcrops in the Longmenshan fold-thrust belt. The Ediacaran rocks are further subdivided into two formations, the Doushantuo Formation of the Lower Ediacaran and Dengying Formation of the Upper Ediacaran (Lambert, Walter, Zang, Lu, & Ma, 1987). Three wells penetrating the acoustic basement beneath the Doushantuo Formation, encountered granites dated to ca. 800 Ma by U-Pb zircon dating (Gu, Zhang, & Yuan, 2014). The stratigraphy and palaeogeography of the Doushantuo Formation is extensively reviewed by Jiang et al (2011) and the majority of the unit is interpreted to be deposited on a rimmed carbonate shelf on the Yangtze shelf. It contains exceptionally well-preserved fossils of multicellular eukaryotes. It is found over extensive areas of the Yangtze block extending significantly to the east of the present-day Sichuan Basin, but there are uncertainties in the paleogeographic reconstruction of some of the sections due to poor exposure and the tectonic complexity of South China. The classic outcrop sections where it has been intensively studied are the Yangtze gorges area (and specifically the section at Wuhe-Gaojiaxi), to the east of the Sichuan Basin and then along a W-E transect through mountainous areas to the SE of the main Sichuan Basin (Jiang, Shi, Zhang, Wang, & Xiao, 2011). Its age is fairly well constrained in comparison to similar age successions elsewhere in the world by U-Pb zircon dates in underlying basement and from ash beds in clastic strata of the Liantuo Formation and Banxi Group which underlie the Doushantuo Formation in outcrops to the east of the Sichuan Basin. Its basal age is 635±0.6 Ma (see references in Jiang, Shi, Zhang, Wang, & Xiao, 2011) and its top is constrained to 551±0.7 Ma from an ash bed near the Doushantuo/Dengying boundary (Condon et al., 2005; Zhang et al., 2005).

In the classic Yangtze gorge area the Doushantuo Formation is about 100 m thick, and is comprised of four members, that include shallow water carbonates, black shales and muddy dolomites. A thin ash layer with U-Pb age of 635.2±0.6 Ma occurs within the lower member (Condon et al., 2005) and is used to date the base of the Formation. Where drilled in the central Sichuan Basin, the Doushantuo Formation in the varies from a few to twenty meters in thickness and is mainly composed of siltstones and sandstones equivalent to the top member in the Yangtze Gorge area. Based on a distinctive negative $\delta^{13}C$ excursion which occurred at ca. 580 Ma between the third and fourth members of the Doushantuo Formation, an age of ca. 580 Ma is used for the base of the Doushantuo Formation in the central Sichuan Basin (Zhu, Zhang, & Yang, 2007; Liu et al., 2014; Zhou, Yuan, Xiao, Chen, & Hua, 2019).

The Dengying Formation, which conformably overlies the Doushantuo Formation, was also mainly deposited on a shallow-water carbonate platform. It too contains abundant fossils, which include Ediacaran-type soft-bodied fossils, trace fossils and macro-algae (Chen et al., 2013, 2014; Yang, Li, Zhu, & Condon, 2017, and references therein). Ash beds in the eastern Yunnan province have yielded a U-Pb zircon age of 546±3 Ma for Member 3 within the Dengying Formation (Yang, Li, Zhu, & Condon, 2017). Using $\delta^{13}C$ isotope correlations, Yang et al. (2017) propose that the top of the Dengying Formation could be c. 541 Ma. The Dengying Formation is characterised by thick microbial dolomites, and is divided into 4 members (Zhu, Zhang, & Yang, 2007; Duda, Zhu, & Reitner, 2016; Zhou, Wang, Yin, Yuan, & Zeng, 2016; Lin, Peng, Du, Yan, & Hou, 2017). Within the Sichuan Basin its lithology is well characterised because it forms the reservoir for important gas discoveries in the central Sichuan Basin including the Weiyan and Anyue fields (e.g. Du et al., 2014; Zhu, Wang, Xie, Xie, & Liu, 2015; Song et al., 2018; Zhai et al., 2020) and has been cored as well as extensively drilled. Member 1 (Z_2dn^1), is 10-50 m thick, and is mainly composed of argillaceous dolomites. Member 2 (Z_2dn^2), which varies between 20 and 1000-m-thick, is characterized by the occurrence of microbial botryoidal dolomite, consisting of laminated dolomite, thrombolite, stromatolite, oncolite and bindstone. The top of Member 2, is defined by a karstified unconformity (Li et al., 2013; Zhou, Wang, Yin, Yuan, & Zeng, 2016; Luo, et al., 2018), but seismic and well data do not suggest that this event was an angular unconformity and most likely represents local variation in sea-level with erosion and the development of a karstified surface. Member 3 (Z_2dn^3), varies from a few centimetres to more than 100 m in thickness, and consists of a varied stratigraphy including interbedded siliciclastic, carbonate rocks and siliceous rocks with volcanic ash interpreted as a mixed shelf sedimentary environment (Deng et al., 2020). Member 4 (Z_2dn^4), which varies from 0-400 m thick, consists of medium-to-thick laminated dolomite, thrombolite, stromatolite, oncolite and bindstone (Li et al., 2013; Duda, Zhu, & Reitner, 2016; Zhou, Wang, Yin, Yuan, & Zeng, 2016; Luo et al., 2018). In the platform areas its top is defined by a flat karstified unconformity, although within the trough there is continuous deposition. The Dengying Formation spans ca. 551-541 Ma, with an age of 546 Ma recorded for Member 3 in equivalent South China outcrops (Condon et al., 2005; Yang, Li, Zhu, & Condon, 2017). The duration of the two unconformities is assumed to be on the order of ~1 Myr (Figure 3).

Until recently it was assumed that platform and lagoon facies dominated throughout the Sichuan Basin (e.g. Yang, Li, Zhu, & Condon, 2017), however on a smaller scale within the Sichuan Basin, significant variations in the Dengying Formation facies has also been noted in the well data drilled during hydrocarbon exploration and production (e.g. Zou et al., 2014; Gu et al., 2016; Zhou et al., 2017) and in particular within the trough where the Dengying Formation is much reduced in thickness and consists of mudstones interbedded with cherts and dolomites deposited in a slope environment (Figure 3). At least 10 wells confirm the presence of slope facies in the Dengying Formation within the trough (Zhou et al., 2017).

The Maidiping, Qiongzhusi, Canglangpu, and Longwangmiao Formations make up the Lower

Cambrian in the Sichuan Basin (Li, Yu, & Deng, 2012; Zhou et al., 2017) (Figure 3). The occurrence of marine fossils within the Lower Cambrian strata has allowed the stratigraphy to be dated by more standard biostratigraphic methods and the ages shown on Figure 3 are those used in the Cambrian chapter of 'The Geologic Time Scale' (Peng, Babcock, & Cooper, 2012) based on the classic Cambrian sections mainly in Hunan Province. The oldest Cambrian Formation, the Maidiping Formation (ca. 541-521 Ma) contains grey carbonates and black shales, with siliceous, phosphoritized dolomite and phosphoritizied micritic limestones, indicating that at least some of its deposition was in an anoxic setting. Small shelly fossils also appear for the first time within the Maidiping Formation. The Maidiping Formation does not have an even thickness or facies distribution across the Sichuan Basin; it is thin in many areas outside the trough and reaches maximum thicknesses of up to ~500 m within the trough (Zhu et al., 2003; Zhou et al., 2017).

The Qiongzhusi Formation (ca. 521-517 Ma), which ranges in thickness from 10s to hundreds of meters, is defined by the first occurrence of trilobites, and mainly consists of organic-rich, black shale and gradually coarsening upward into muddy siltstones and siltstones (Zhu et al., 2003; Li, Yu, & Deng, 2012; Zhou et al., 2017). It is considered to be an important source rock for Upper Ediacaran to Cambrian hydrocarbon reservoirs of the Sichuan Basin. It too reaches its maximum thickness in the trough and is interpreted to be deposited in a deeper water slope to basin environment. Above the Qiongzhusi Formation the Canglangpu Formation (ca. 517-511 Ma), is relatively thin, and is ～200 m in thickness. It consists of medium thick marine sandstones and siltstones. There is a ～30 m thick limestone unit in the middle of the formation which forms a regional correlation event that can be identified on seismic data (Li, Yu, & Deng, 2012; Shen, Hu, Pan, & She, 2017; Figure 4). It marks a return to a more open, shallow-marine depositional environment (Zhou et al., 2017).

The overlying Longwangmiao Formation (ca. 511-509 Ma), which reaches a maximum thickness of 150 m, consists mainly of dolomitised limestone, with lesser amounts of argillaceous and sandy dolomites and a thin interval of siliciclastic rocks in the middle of the succession. These lithofacies are consistent with renewed shallow water deposition on a carbonate platform, with shoals and local development of lagoons (Gu et al., 2016; Ren et al., 2017; Shen, Hu, Pan, & She, 2017). By Longwangmiao times there is no evidence for deeper depositional environments within the trough. Above the Longwangmiao Fomation, the Middle Cambrian Douposi Formation ranges from 10s to 200 metres in thickness and consists of mixed clastic rocks, carbonates and evaporites, deposited in shallow water environments. Due to later tectonic uplift between the Late Ordovician and Devonian, the Douposi Formation and Upper Cambrian has been eroded in the centre and south west of the Sichuan Basin.

3 DATA AND METHODOLOGY

3.1 Seismic Data

A very large dataset of 3.78×10^4 km of regional 2-D seismic reflection lines, and ～3×10^4 km^2 3-D seismic reflection volumes of varying vintages and resolution were used for the study. For the key intervals pertinent to the study the frequency content of the seismic data gives a vertical resolution of 58 m for the Dengying Formation, 44 m for the Lower Cambrian and 48 m for the Middle Cambrian to Ordovician. The data are positive polarity, where a black event is a positive amplitude in seismic sections (Figures 4-7).

The isochron maps were converted to thickness, or isopach, maps using seismic velocities of 6500m/s for the Dengying Formation and 5500 m/s for the Lower Cambrian Formations. An extensive well data base, including core and wireline logs were used for lithology interpretation and the construction of the palaeogeography maps. Twelve of these wells located on the margins, and within the trough as well as more widely distributed within the Sichuan Basin were used for the subsidence analysis. We also used a further 6 locations within the basin where stratigraphic columns ('pseudo' wells) were constructed from seismic data combined with well data. These are labelled PS1-6 (Figure 2). Our intention was to capture any signal of the trough within the subsidence analyses and to be able to compare the trough subsidence with the subsidence patterns more regionally within the basin. To convert the seismic travel times to depth for the pseudo-wells velocities of 3500-4500 m/s were used for surface to Upper Triassic; 5000-5500 m/s for Middle Triassic to Permian carbonates and for the Cambrian 5500 m/s.

3.2 Subsidence analysis

The well, and pseudo-well, data were backstripped using the standard approach of Steckler and Watts (1978) and Sclater and Christie (1980). It is a technique well established in basin analysis and further details on the method can be found in text books such as Allen and Allen (2013). The sedimentary column is first decompacted which requires knowledge of porosity variation as a function of depth. The decompacted sedimentary column is then converted from a sediment to a water load (Steckler & Watts, 1978); this two-stage approach provides water-loaded basement subsidence through time. At each time - step, the depth of the basement (or total subsidence, S) is calculated by summing the decompacted thicknesses of the deposited units with corrections for palaeowater depths. We assumed Airy isostasy for our work, as has been done by many previous authors (e.g. Barton & Wood, 1984; Xie & Heller, 2009; Berra & Carminati, 2010, amongst many others) and given the large uncertainties in current knowledge of lithosphere properties beneath the South China craton in the late Neoproterozoic and Cambrian this seems a justifiable approach.

For backstripping, data is required on the ages, lithologies and palaoewater depths of the sedimentary units in the stratigraphic column. Different rock types compact at different rates and have different densities which also varies as a function of porosity; thus appropriate parameters have to be assigned to the lithologies to allow for accurate decompaction and loading calculations. Although there are more sophisticated approaches for estimating the reduction in porosity with depth through a sedimentary section, by including sediment compressibility and permeability variations through time as proposed by Audet and McConnell (1992) for example, for most backstripping studies the modelling of decompaction using an exponential porosity-depth relationship had been found to suffice, because it is the large-scale porosity reduction trends in the subsurface that we seek to model (Bond & Kominz, 1984; Berra & Carminati, 2010). We use the following equation (Athy, 1930)

$$\emptyset = \emptyset_0 e^{-cz}$$

where ϕ is the porosity at depth z, ϕ_o is the porosity of sediments at the surface and c is an empirically derived compaction coefficient that varies with lithology. Decompaction parameters and rock grain densities in the literature usually refer to single lithologies and those we have chosen to use are shown in Table 1. Ideally one would fit a trend to porosity data collected from wireline logs within a basin to calculate a basin-specific compaction trends. We were unable to do this for our study, so used 'standard' parameters of Sclater and Christie (1980) for clastic rocks. For carbonate lithologies we chose to use the parameters published by Schmoker and Halley (1982). These authors compared a large dataset of both near surface Holocene, and older, denser Mesozoic carbonates in Florida to construct porosity reduction trends for limestones and dolomites. Subsequently Bond and Kominz (1984) who reconstructed the tectonic subsidence in the Canadian Rocky mountains for early Palaeozoic rocks containing substantial thicknesses of carbonate rocks found that their curves gave similar results to those proposed by Schmoker and Halley (1982). To further assess the robustness of using the Schmoker and Halley (1982) parameters we compared them with the compilation of compaction trends made by Giles (1997). Giles (1997) summarises a range of published compaction datasets and limestones in particular demonstrate a large variation with depth where the initial porosity can vary from 20 to 80% decreasing to values of between 0 and 10% at 6 km depth. The Schmoker and Halley (1982) curve plots midway within the distribution of Giles (1997) and hence we consider it to be adequate for our purposes. For formations or units with mixed lithologies the decompaction parameters and grain densities are calculated by arithmetically averaging, according to the proportion of each lithology, the parameters for the single lithologies given in Table 1.

Palaeowater depth estimates are an important source of potential error in subsidence analysis (e.g. Bertram & Milton, 1989) and we have assigned minimum and maximum water depths based on the facies and palaeogeographic analyses. For the shallow water platform carbonates that dominated the Upper Ediacaran and Cambrian and the shallow water sandstones of the Doushantuo and Canglangpu Formations water depths of less than 30m are appropriate and we used 25±25m for the modelling. Estimating a palaeowater depth for rocks deposited within the trough is more problematic and we discuss this further below.

Another important potential error to consider are the ages assigned to the lithostratigraphic units, as the age points control the slope of the backstripped subsidence curve. As discussed above assigning absolute ages to the Ediacaran and Cambrian for the Sichuan Basin is challenging. The Ediacaran is constrained by some radiometric ages but the Cambrian is largely dated by long-distance lithostratigraphic correlations to classic sections further east on the craton. For the Doushantuo and Dengying Formations we have attempted to use the best documented geochronological ages that we could find in the published literature. In Figure 3, inferred ages, as used in the regional and local Chinese literature are shown preceded by '~'. The Cambrian Formations in the Sichuan Basin are more reliably dated with lithostratigraphic correlations to classic sections in Hunan Province (e.g. Zhu et al., 2003; Li, Yu, & Deng, 2012) using the ages of Peng et al. (2012). We used the new International Chronostratigraphic Chart from ICS (Cohen, Harper, & Gibbard, 2018) to assign ages to Cambrian divisions. For the backstripping we divided the Ediacaran to Lower Cambrian succession into nine units based on the age control available, the lithologies and unconformities and significant variations in paleobathymetry, as discussed above. From bottom to top, the nine stratigraphic units are the Doushantuo Formation, Z_2dn^{1-2}, Z_2dn^3, Z_2dn^4, Maidiping, Qiongzhusi, Canglangpu, Longwangmiao, and Douposi Formations. The unconformities identified (Figure 3) are considered to be of short duration and as there does not appear to be any significant erosion at these intervals at a scale that will affect the tectonic subsidence, they have not been modelled. The unconformities are identified in the platform and shallow water areas and cannot be traced into the trough where the sedimentation is thought to be continuous.

Given the uncertainties in the long-term global eustatic curves, and particularly in Neoproterozoic and Cambrian terms we have made no eustatic sea level corrections (Watts, 1982). This approach is consistent with that of other backstripping studies (e.g. Barton & Woods, 1984; Xie & Heller, 2009; Berra & Carminati, 2009). Any errors from omitting modelling of any potential sea level variations are likely to be less than other possible errors as discussed above. We used BasinVis 1.0 (Lee et al., 2016) for calculating the water-loaded tectonic subsidence, which uses the Steckler and Watts (1978) equations.

TABLE 1 Porosity parameters and grain densities used in this study

Lithology	Porosity at the surface (ϕ_o)	Compaction coefficient, c, (km^{-1})	Grain density (kg/m^3)	References
Sandstone	0.49	0.27	2650	Sclater and Christie (1980)
Shale	0.63	0.51	2675	Sclater and Christie (1980)

Limestone	0.513	0.518	2710	Schmoker and Halley (1982)
Dolomite	0.303	0.216	2870	Schmoker and Halley (1982)

4 RESULTS

4.1 Seismic interpretation

4.1.1 Intraplatform trough geometry

We use several key pieces of evidence to map the geometry and document the palaeogeographic significance of the Upper Ediacaran to Lower Cambrian SE-NW oriented trough in the Sichuan Basin. Firstly, the trough margins are well-imaged on seismic data, despite being currently located at depths of more than 8 km within the basin (Figures 4-7). Secondly with detailed, new, regional mapping of the Dengying Formation members, and the Lower Cambrian Formations on seismic data, where the seismic markers have been tied accurately to well data, the shape of the trough and location of the platform margins can be seen on thickness maps (Figure 8). The trough extends from NW to SE, with a width of 50 km in the SE and expanding to the NW and reaching a width of ~200 km before being buried or deformed within the Longmenshan (Figures 2 and 8). We have chosen 5 seismic sections from 3-D surveys, A-E on Figure 2, perpendicular to the trough margins with which to illustrate the margin and fill geometries (Figures 4-7). Sections A to D are from the eastern margin of the trough; and E is located on the western margin.

The second piece of evidence is the isopach maps (Figure 8) which document significant thickness changes in the Upper Ediacaran and Lower Cambrian Formations. The isopach maps illustrate that the trough margins are not only sharp, but also that the platform margin location changes through time, backstepping as it becomes younger (Figures 4-7 and 8c).

Section A, across the northern part of the trough, shows the stratigraphic succession from the basement to Permian (Figure 4). Two shelf margins are imaged, the most westerly of which lies beneath the frontal fold and thrust belt of the Longmenshan deformed post-Middle Triassic times. Although there is no well drilled into the basement in this area, it is inferred to lie below the lowest strong impedance reflection at ~ 3750 ms Twtt on the NW side of the section. The Doushantuo Formation is interpreted to lie between the two strong impedance reflections between ~3650 and ~3750 ms TWtt on the NW of the section. Within the overlying Dengying Formation there are considerable thickness changes due to the development of the trough. The early Late Ediacaran strata of the lower two members of Dengying Formation (Z_2dn^{1-2}), are characterized by the sharp thinning (less than 50m-thick) in the trough and thickening to over 1000 m on the SE side of the section. Another sharp edge with thickness changes in the upper two members of Dengying Formation can be seen some 40 km further to the SE. The maximum thickness reached by Members

3 and 4 in the trough is ~50m, were as on the platform the thickness reaches 350-400m (Figure 8c). The unconformity defining the top of the youngest Denying Formation member (Z_2dn^4t) has a strong impedance contrast with the overlying, lower velocity, Cambrian shales. The seismic data show that the lowermost 200ms twt (~550m) of Cambrian strata only (the Maidiping and Qiongzhusi Formations) are deposited in the trough and are missing on the platform. Onlap within the Maidiping and Qiongzhusi Formations is observed in front of the older platform margin, and after burial of the first platform edge more onlap can be seen in front of the younger back-stepped platform margin. By Canglangpu Formation times the trough was completely filled (Figures 4, 6 and 7). A single isopach map has been produced for the Lower Cambrian to the marker limestone within the Canglangpu Formation (Figure 8d). Within the trough the Lower Cambrian varies from ~600m thickness in its the narrower southernmost parts to between 1500 and 2000 m in thickness in the west and north west. On the platform, the Lower Cambrian in general does not reach more than ~100m in thickness. The remaining Lower Cambrian to the Middle Cambrian is largely isopachous within the study area (Figures 4, 6, 7).

Aside from faults associated with the Longmenshan folds in the northwest of the section that detach within the Cambrian, and hence do not deform the Upper Ediacaran and Lower Cambrian of our study, there are no obvious faults seen from section A (Figure 4). There is however a zone of apparent seismic discontinuity at the position of the younger Dengying Formation platform margin. Because the data are displayed with a large vertical exaggeration the image is misleading and when the seismic data are displayed at true scale (Figure 5b) there are no faults located at, or below the platform margin.

On sections B, C and D (Figure 6) located at the narrowest part of the trough the younger platform margin is well-imaged, and has a similar height (~90 ms Twtt) to that seen on Section A. The older platform edge can also be identified on the seismic data; on section B it is ~6 km outboard of the younger margin; in section C, it is located ~4 km inboard of the younger margin, and in section D a similar distance outboard. In general, the thickness changes from the platform to the slope for the older margin over a distance of 10 km are more gradual for Members 1 and 2 of the Dengying Formation, than for the younger Member 4 (see also the isopach map in Figure 8c). However, the isopach maps show that when integrating all the seismic data, both platform margins can be mapped continuously on the eastern side of the trough and that at this seismic resolution the younger platform has a steeper gradient (Figures 8b, c). Some faults offset the Dengying Formation in sections B and C; these are part of a regional fault system that develops in Permian times and appear not to be related to the development of the trough. We show one seismic section, E, that images the lower platform margin on the western margin of the trough. In places the margin edge is not as sharp a feature as in some locations on the eastern margin; For example, in section E (Figure 7) a gradual thickening of Members 1 and 2, from 24 km to 14 km towards the platform occurs over a distance of

~10 km. We use the limit of onlap of the Lower Cambrian strata to the SW onto the relict margin palaeobathymetry, to define the most landward position of the platform edge (arrowed in Figure 7). In other datasets the margin is more pronounced and again when all the data are collated on an isopach map a platform margin can be identified fringing the entire trough.

Integrating well and outcrop data with regional mapping suggests that the younger platform margin has back-stepped significantly in the south of basin; we find evidence of platform facies, with microbalities in both Members 2 and 4 of the Dengying Formation in well LL1 (Figure 9) and hence infer that the platform margin lies somewhere to the west of well W117 which only encountered one cycle of platform carbonate. The position of the younger margin does not show up in the Member 4 isopach map because there is only 2-D seismic data coverage in the SW of the basin, and the quality does not allow for accurate mapping of the margin, hence we depict with a dashed line on relevant maps.

4.1.2 Platform margin geometry

Figure 5 illustrates the two platform margins of section A at near 1:1 scale. The older of the two margins (Figure 5a) has many features of a carbonate, reef-fringed platform margin; it has a slope dip of ~20-30° shallowing basinward and appears to consist of at least two vertically stacked mounds separated by a unit of disrupted amplitudes that we interpret as talus deposits. The width of the margin from the mounded top to distal end of the talus deposit is ~4 km and the vertical relief on the uppermost platform edge is ~250 ±58 m. The mounded top visible on the lower platform edge suggest that it may have been a rimmed shelf. Well data along the margin confirm that the margin mounds are composed of microbial mounds with carbonate shoals (Figures 9, 10). The second platform margin (Figure 5b) is also defined by a well-developed mound, with a strong amplitude reflection defining a flat base, overlain by a 1.5 km wide lens of lower amplitudes enclosing a dipping surface (clinoform?). Landward (eastwards) the lens passes laterally into parallel amplitudes of gypsum-bearing dolomites deposited in a lagoon (Figure 10). The vertical relief on this platform is ~200 ±58 m. The top of the mounded is defined by a strong amplitude event which is the karstified top of the Dengying Formation. On section C, the youngest platform margin appears to build basinward with the development of a lensoid unit with clinoforms in its lower part (see arrow on Figure 6b). The height of the front of the lens is ~300 ±58 m. Likewise, on section D a low amplitude thin lens can be observed at the younger margin (Figure 6d); The lens is of a similar height to that imaged on section C with a width of ~ 3 km.

In summary, the seismic data allow us to interpret sharp platform margins associated with lensoid, clinoform and mounded geometries, with heights that range from 150 to 300±58 m, which appear to be best developed for the youngest platform margin. On at least one of the sections talus shed from the margin is visible. The well data (Figure 9) confirm that the margins are made up of microbial mounds, with fringing shoals outboard of dolomitic lagoons. Given the vertical limit of the seismic resolution the heights calculated for the platform margins may well be an upper bound, and we cannot discount that the margins were actually shallower features that grew predominantly by vertically stacking. Assessing the height of the platform edge is an important constraint for estimating the palaeowater depth for the ramp and slope facies in the trough. Values for heights of platform margins of around 200-300 ± 50m are the same order of magnitude as those documented for other Ediacaran platforms in Namibia, Oman and on the eastern edge of the Yangtze platform in China (Adams, Schroder, Grotzinger, & McCormick, 2004; Verhnet & Reijmer, 2010; Grotzinger, & Al-Rawahi, 2016). The dominance of algal/microbial mound builders on Ediacaran platforms, would have promoted stabilisation of the platform allowing thick platforms with steep margins to form. Hence, we use a water depth range of 150-350 m for the Dengying Formation for the subsidence analysis for locations within the trough.

4.2 Well correlation and palaeogeography

4.2.1 Well correlation

A SW-NE trending well correlation panel perpendicular to the trough has been constructed through wells LL1 - W117 - Z4 - ZY1 - MX9 - MX11 - MX39 which illustrates the lithology and facies changes within the Dengying and lower Cambrian Formations (Figure 9). The correlation panel shows considerable thickness and lithology variations from the trough to the platform margins in the upper Ediacaran and Lower Cambrian rocks, and provides valuable further information about the facies that developed during these times.

Members 1 and 2 of the Dengying Formation (Z_2dn^{1-2}) thin from more than 500 m in the platform to less than 50 m in the trough. In wells LL1 and W117, Z_2dn^{1-2} is about 600 m thick, and consists of botryoidal laminated dolostone of intraplatform microbial reef and mound facies, calcareous micritic dolostone and argillaceous gypsum of evaporite tidal flat facies. The Z4 well, which lies in the western margin of the trough during Members 1 and 2 times, encountered various microbialite dolostones in the upper part of the Z_2dn^{1-2}. In contrast well ZY1 consists of c. 50m of interbedded microbialite dolostone and micritic limestone consistent with a slope environment. Wells MX9 and MX11 on the eastern platform encountered various microbialite dolostones of intraplatform buildups and micritic dolostone but did not reach the bottom of Z_2dn.

Member 3 of the Dengying Formation is generally much thinner than Member 2 and is dominated by mixed carbonate and siliciclastic rocks both in the trough and on the platform. In wells LL1, W117 and Z4 on the western platform, Z_2dn^3 is less than 2 m thick and the lithology is mainly blue gray mudstone. On the eastern platform wells MX9 and MX11 encountered a thicker section of Member

3, composed of interbedded sandstone, mudstone and carbonate rocks. The two trough wells, Z4 and ZY1 consist of thin sections (<25 m) of mudstones and argillaceous dolomite.

Within the trough Member 4 (Z_2dn^4) consists of ~20-50 m of interbedded argillaceous dolomites, indicating deeper water deposition (wells Z4 and ZY1). However, on the platforms the thickness of Member 4 increases dramatically. In wells MX9, MX11 and MX39 on the eastern platform, Z_2dn^4 is ~ 300-400 m and is dominated by microbial dolostones similar to the Member 2 facies. Similarly, on the western margin, the thickness increased from several meters of dolostone in well W117 to more than 200 m of dolostone and microbialites in well LL1.

The Lower Cambrian Maidiping and Qiongzhusi Formations filled the trough and onlapped the platform margins (Figure 9). The thickness decreased from more than 600 m in the trough as shown in ZY1 to 100~200 m on the platform as shown in wells LL1 and MX9, MX11 and MX39.The Maidiping Formation mainly consists of dolomites some of which is phosphoritic in the shelfal wells, and argillaceous carbonates, cherts and shales in the deeper trough. Black shales, siltstones and sandy mudstones form the Qiongzhusi Formation in the trough, likewise deposited in a deeper water environment.

Two unconformities can be recognized in the platform wells, the older of which occurs at the top of the Member 2 of the Dengying Formation and the younger at the top of Member 4 of the Dengying Formation. The unconformities are not traceable in the trough. The unconformities are karstified and represent two periods of emergence of the platform. We have no estimates of the amounts of potential erosion at these unconformities.

From the well correlation, three conclusions can be drawn: (1) deposition within the trough was continuous from the Late Ediacaran to Early Cambrian; (2) Considerable backstepping of the platform occurred during Member 4 of the Dengying Formation, particularly on the western side of the trough; and (3) there are two karstified unconformites at the top of each platform interval which indicates emergence.

4.2.2 Palaeogeography

Based on the integrated analyses of the seismic interpretation, well correlation and outcrop data, two palaeogeography maps for Members 2 and 4 of the Dengying Formation, at platform margins times, have been constructed. Given the extensive well database, and the identification of the platform margin location from the seismic data, we can derive a detailed understanding of the palaeogeography in late Ediacaran times. Microbial reef-mounds with carbonate shoals formed both on the platform margin and on open platform regions; lagoons with gypsum bearing dolomites or anhydrites and inter-mound/bank facies are identified and mapped (Figures 10a, b). The platform passes laterally into an open water slope and eventually basin facies in the west. Photographs of both outcrop and core of these facies are illustrated in Zhou et al. (2017) and Zhu et al. (2015).

During the early Late Ediacaran (Member 2 of the Dengying Formation) the NW-SE trending trough is fringed by microbial reefs and shoals forming long, narrow belts (Figure 10a). Specific reefal lithofacies drilled in 5 wells through the platform margin facies include microbial framestone with thrombolite, spherulite, spongiostrome, stromatolites and laminate structures. Dolostones consisting of oncolite, ooids, and gravels make up the shoal facies. The Ediacaran reefs fringe a platform dominated by open marine conditions with smaller isolated microbial mounds and shoals. Directly inboard of the platform margin reefs, more restricted lagoonal conditions existed where playa-style deposits formed. In Member 2 times the embayment, defined by the fringing microbial reefs, is narrow in the south widening to the NW and we interpret that slope facies developed in the embayment, passing into deeper water in the region of the present-day Longmenshan.

In Member 4 times very similar facies were developed, and on the eastern side of the open sea the platform margin is again well-developed as a narrow, N-S striking continuous belt of microbial reefs and beach shoals; it has back-stepped with respect to its location in earlier Member 2 times, and has changed orientation, from a NE-SW strike in Member 2 times to N-S. The wells drilled through this unit encountered very similar microbial framestones to Member 2, but without botryoidal lamination. Wells in the northern and central Sichuan Basin encountered lagoonal facies behind the platform margin characterized by black-gray gypsiferous micritic dolomite, dolomites and evaporites (Figure 10b). However, the main difference at Member 4 times is that the platform margin on the west of the trough has back-stepped significantly, by up 100 km southwards in some areas (compare facies at well W117 in Figure 10a and b). For example, at Member 2 times, a platform margin existed underneath Chengdu, but by Member 4 times Chengdu would have been located in deep water. Well data, outcrop and seismic data were used to support the proposed location of the platform at Member 4 times in the SW of the study area as shown on Figures 8c and 10b. We think that a narrow embayment occurred along the platform margin, but further south with respect to its location at Member 2 times. We interpret the presence of karstified surfaces at the top of Members 2 and 4 platforms to indicate that there were periods of sea-level fall and emergence of the platform.

We note that these new palaeogeography maps differ from those published by Zhou et al. (2017). The principal reason is that these authors did not recognize the presence of the Member 2 platform margin and only identified an N-S trending trough that developed in Member 4 times. They consider that the karstic surfaces that developed at the top of Members 2 and 4 were associated with uplift events in the hinterland to the Sichuan Basin and that erosion associated with these events led to 'downcutting' and formation of the trough.

5 TECTONIC SUBSIDENCE

We have backstripped the entire sedimentary fill of the basin for Well GS1 located in the centre of the basin to illustrate how the main tectonic events known to have affected the Sichuan Basin can be identified by subsidence analysis (Figure 11). The decompacted basement burial curve is shown in blue and the water-loaded, backstripped, subsidence is shown in red, with pale blue error bars for the range in estimated palaeowater depth. The curve shows an initial rapid increase in subsidence in Ediacaran times, and two further larger magnitude subsidence events in the Permian and upper Triassic to Tertiary. From the curve four tectonic periods can be identified: Firstly, rapid linear subsidence of < 0.5 km in Ediacaran time, decaying to a slower rate of subsidence through to middle Ordovician time, which exhibits the typical shape of subsidence due to lithospheric extension. Secondly, the late Ordovician to Carboniferous is a time of uplift and erosion known as the Caledonian or Guangxi event. The evidence for this is a regional, low-angle erosional unconformity mappable in the centre and west of the Sichuan Basin that eroded Middle Cambrian to Ordovician strata. However, we do not include estimates of the missing sections that have been eroded in the modelling, as this was beyond the scope of the study. A second period of rapid subsidence of ~500 m occurred from Permian to Middle Triassic which is a response to regional extension with the Sichuan Basin. The Sichuan Basin was located in a passive margin position on the edge of a Palaeoasian ocean (e.g. Torsvik & Cocks, 2017) and a hot spot that produced the Emeishan flood basalts is located to the south of the Sichuan Basin at this time; 100-200 m of basalts have been drilled in wells in the SW Sichuan Basin. Fourthly the collision of the North and South China cratons, with closure of oceans to west and north of the Sichuan Basin led to formation of the fringing mountain belts and the associated foreland basin cycle within the Sichuan Basin. This is expressed by 2-4 km of tectonic subsidence from late Triassic to ~40 Ma. We use the data in Richardson et al. (2008) to extrapolate a semi-quantitative estimate of what the maximum foreland basin subsidence might have been assuming 4 km of erosion of late Jurassic to Tertiary sediments in the last 40 Ma.

A further 18 backstripped subsidence curves for the Ediacaran to middle Ordovician stratigraphy of the Sichuan Basin are shown in Figure 12. Twelve are calculated from well data and the remaining 6 for ‘pseudo-well’ locations based on wells and interpreted seismic data to extend the stratigraphy beneath the wells (Figure 8). As discussed in previous sections the Ediacaran water depths are well-constrained for platform regions, and we have used the depth-converted heights of the platform margin measured from seismic data to give a palaeowater depth range for the trough wells for the Ediacaran and lower Cambrian strata. The average palaeowater depth is shown by the filled pale-blue curve on the graphs, and error bars for the water-loaded backstripped tectonic subsidence, due to the range given for the palaeowater depths are in green on the red tectonic subsidence curve. For 11 of the 18 curves there is little to no subsidence recorded from ~510 Ma (Middle Cambrian) to 444 Ma (Ordovician) because of the regional erosion in the centre and south west of the basin as described above. In the majority of locations, and particularly in shelfal locations, two linear increases in subsidence rate are seen, the first at ~551-541 Ma coinciding with the deposition of the Dengying Formation and the second in the early Cambrian starting with the onset of deposition within the Qiongzhusi Formation (~521 Ma). Between these two events there is a period of ~ 20 Ma when the subsidence decreased or halted which coincides with the unconformity at the top of the Dengying Formation and the duration of the Maidiping Formation. This hiatus is most pronounced in the shelfal wells where the thickness of the Maidiping Formation is at most 10s of metres (Figure 9) but is missing in the trough wells where thicknesses of the Maidiping Formation reach a few 100 metres. The first of these episodes records a modest amount of tectonic subsidence varying from less than 300 m (e.g. wells HT1 and ZS1) to over 600 m in the wells in the NW (e.g. LT1, PS2, PS5 and PS6). The 7 wells that have stratigraphy continuing throughout the Cambrian are particularly important because they give an insight into the Cambrian subsidence episode. They show that the early Cambrian period of increased linear subsidence then declines slowly over ~70 Ma, with a shape typical of basin formed by lithospheric extension followed by thermal cooling. Well GS1 (platform margin well) has a total amount of ~200 m of tectonic subsidence in the Cambrian and this increases to 700-800 m for wells such at HT1 and ZS1. It is clear that if the wells in the west such as PS5 and PS6 were to follow the same trend they would have more subsidence than the ~500 m currently recorded for the early Cambrian up until ~510 Ma.

We have contoured the tectonic subsidence for the 12 wells and 6 pseudo-wells in order to investigate the spatial variation in the water-loaded subsidence and present the results for 4 intervals, which are the Doushantuo Formation (earliest deposition on basement), Members 1 and 2 of the Dengying Formation, Member 4 of Dengying Formation and the early Cambrian Maidiping and Qiongzhushi Formations (Figure 13). Each map illustrates the cumulative total subsidence up to that time. The subsidence at Doushantuo times is very low and varies between 50 and 200 m. The largest increases occur in Dengying times (Figures 13b, c), with a modest increase varying from 100 to 500 m in the Early Cambrian (Figure 13d). Although this last map only represents the initial phases of the Cambrian subsidence, it at least gives an idea of how the Cambrian episode starts. All four maps show that the tectonic subsidence increases to the west and north towards the Longmenshan and the Micangshan fold and thrust belts. There are some local variations, most notable in Cambrian times where there is a deflection of the contours towards the south in the apex of the final position of the back-stepped platform margin. However, the most striking conclusion from the contoured tectonic subsidence is that any increase in subsidence does not coincide with the location of the deeper water sedimentary environments, and therefore strongly suggests that the palaeogeograhy of the Ediacaran carbonate platform, with the embayment (the trough) along the margin is not tectonically controlled. This is consistent with the lack of any underlying or contemporaneous faults at the platform margin noted from the comprehensive analysis of the seismic data. There is of course, always the possibility that there are normal faults that are not imaged because they are beneath the seismic resolution. These would have to be very small faults of throws between 100-150m given that the vertical resolution of the 3-D data is ~58m.

We have constructed a 2-D cross-section from the contoured tectonic subsidence in the northern part of the study area from ESE to WNW that crosses the location of both platform margins (Figure 14). The subsidence for each time interval is plotted and illustrates how the subsidence has varied smoothly from the basin interior to the west with a broad, gentle deflection of the basement (shown by red line on Figures 14b, c). Viewing the subsidence results in this way also makes it clear that there is no increase in tectonic subsidence associated with the position of the platform margin. This backstripped section is consistent with the thickness maps of the Dengying Formation (Figures 8b, and c) where total thicknesses of up to 1500 m of carbonates accumulated on the Upper Ediacaran platform decreased to values of ~200 m in the west. We would expect that the accommodation space required for 1500 m of carbonates would be the largest signal in the backstripped subsidence, and that filling the trough with up to 400 m of water with very little deposition of Dengying Formation does not compensate for this. The increase in sediment thickness (500-1550 m of mostly shales) deposited in the Lower Cambrian does reflect an increase in tectonic subsidence rate as seen from the individual tectonic subsidence graphs, but because the Lower Cambrian is also deposited outside the trough the change in gradient in the tectonic subsidence is also gentle and likewise does not coincide with the carbonate platform margin. The onset of change in gradient of Cambrian subsidence has moved further west by ~50 km compared to Ediacaran times (see arrow on Figure 14d).

6 DISCUSSION

6.1 Tectonic subsidence -implications for the origin of the Sichuan Basin

In general, the shape of the backstripped subsidence curves would appear to most closely resemble those generated by models of lithospheric extension with two episodes of more rapid extension followed by slower, longer-lived thermal cooling as evident in the wells not affected by the Late Ordovician uplift and erosion. Wells in the northwest of the area (PS6, PS5) and GS17 in the trough record one main subsidence event. To investigate whether the backstripped tectonic subsidence curves from the Sichuan Basin can be interpreted in the context of theoretical models of lithospheric extension (e.g. McKenzie, 1978) or variants with slow strain rates which may be more appropriate for cratonic basins (e.g. Armitage & Allen, 2010) we compare a selection of the backstripped wells with theoretical models (Figure 15). We select 4 curves with the longest history and two wells from the NW of the area where the total subsidence is highest and overlay them on two theoretical models from Armitage and Allen (2010) which use a 200 km thick lithosphere, a crustal thickness of 40 km, with a basal temperature of 1330°C and thermal relaxation of more than 250 Ma. The thickness of the lithosphere in these models makes them appropriate for the location of the Sichuan Basin on the

South China craton, where the lithosphere is estimated to be ~200 km thick (Priestley & McKenzie, 2013). The first model is for instantaneous extension (grey lines in Figure 15) and the second is for finite extension at low strain rates of 10^{-15} s^{-1} (black dashed lines, Figure 15). Because models of instantaneous extension are only appropriate for extension at strain rates greater than 10^{-15} s^{-1} (Jarvis & McKenzie, 1980) the second model at low strain rates is to test the possibility that the Sichuan Basin may have formed as a cratonic basin. The theoretical models do not fit the two episodes of increased subsidence in the shelfal wells, as is to be expected because the models were not run with two closely spaced episodes of short-duration extension. However, the subsidence history of the two wells in the basinal setting, PS6 and GS17, where there is a single episode of more rapid subsidence, can be explained by the theoretical curves. GS17 can be explained by instantaneous extension with a stretching factor of 1.2, and PS6, lies between the theoretical curves for instantaneous extension with a stretching factor of 1.4, and slow strain rate extension with a stretching factor of 1.3. The thermal cooling part of the other wells lie closest to an instantaneous model with stretching factors of 1.2. These results suggest that in broad terms the backstripped, water-loaded, subsidence for wells in the Sichuan Basin is consistent with formation by lithospheric extension and subsequent cooling of cratonic lithosphere starting at ~550 Ma and lasting through the Cambrian until 450 Ma. The amount of lithospheric extension was low with a stretching factor of ~1.2 but increases in the NW part of the study area where it reaches 1.3-1.4 (wells LT1 and PS6). Despite extensive mapping of the Ediacaran and Cambrian strata on an extensive suite of 2-D and 3-D seismic data, there is no evidence for major normal faults and syn-rift depocentres, which would be expected in basins that form by lithospheric extension; this remains a puzzle. A lack of normal faults and associated syn-rift stratigraphy is not restricted to the Sichuan Basin, but is a feature of some other basins such as the Michigan and Williston cratonic basins. Armitage and Allen (2010) show that slow extension of relatively thick continental lithosphere is a mechanism for generating permanent, long-lived thermal subsidence in cratonic basins and to explain the lack of faulting they suggest that at low strain rates the deformation might not localize on large faults. It may be that such as mechanism is also applicable to the Sichuan Basin.

There are other models that might generate similar tectonic subsidence curves, and that do so without the need for the thinning of crust through stretching and the formation of normal faults. One such model is that proposed by Tozer et al. (2017) for the Parnaíba basin and then extended by Watts et al. (2018) to the Congo and Michigan basins. These authors propose that a large area of lower crust that has been intruded by a mafic magmatic body could provide a buried sub-surface load which causes a surface flexure in which sediment accumulates. For the Parnaíba basin, a mid-crustal reflector that extends for ~250 km is visible on a seismic reflection profile that extends across the basin provides observational evidence for such a body. Gravity modelling of the positive, long-wavelength, Bouguer gravity anomaly across the basin is also consistent with such a high density body. We are aware of one published deep seismic reflection line extending from NW to SE across the centre of the Sichuan Basin (Gao et al., 2016). This line images the sedimentary layers of the basin extending to a maximum of 15 km in front of the Longmenshan, the Moho at a depth of 40-45 km, and a SE dipping event that extends beneath the Moho, which the authors propose is the remnant of SE-directed Neoproterozoic subduction. The reflectors that extend beneath the Moho are offset by ~100 km to the east from where we document the largest amount of Ediacaran to Cambrian subsidence, and so we think it unlikely that a relict subduction zone provided a buried load and that any associated related dynamic topography contributed to the formation of the early phases of the Sichuan Basin. However, given the uncertainties in plate tectonic reconstructions for the Neoproterozoic South China area, including where any arcs might be located (e.g. Zhao & Cawood; 2012; Cawood et al., 2018) we consider that it is beyond the scope of this paper to speculate further. Returning to the existence of a potential sub-surface load within the lower crust, there are no seismic events that might indicate a mafic body in the lower crust, though the imaging is poor particularly under the thickest parts of the basin. On balance, with current data available, we have no reason to propose that lower crustal mafic material might have contributed to the subsidence observed in the early phase of basin formation.

A second model that warrants consideration is that of McKenzie and Priestley (2016). These authors have proposed that if the crust is thickened by about 35-40 km and is followed by rapid surface erosion of a similar thickness of upper crust over 10s of Myrs, then the decay of the resultant thermal anomaly will lead to subsidence forming a basin underlain by thick lithosphere. McKenzie and Tribaldos (2018) show how such a model could fit the subsidence curves for the Parnaíba basin. However, in the South China craton there is no evidence in support of an orogenic event that could have thickened the crust and upper mantle in South China in the 125 Ma prior to the formation of the Sichuan Basin. The growing consensus is that in that particular time interval (~820-700 Ma) South China was affected by extension and magmatism associated with the break-up of Rodinia (e,g. Wang & Li,2003; Wang et al., 2021). Most authors favour the cessation of subduction and accretion by 820 Ma (Cawood, Wang, Xu, & Zhao, 2013).

The occurrence of magmatism some 125 Ma prior to the onset of subsidence in the Sichuan Basin suggests that the potential role of thermal models related to mantle plumes should also be considered. The emerging consensus is that between ~800-700 Ma South China lay in a marginal position on the Rodinia supercontinent, close to NW India, and thus would have been a long way from the Rodinia mantle plume (Wang et al., 2021). Nevertheless the Neoproterozoic bimodal magmatism within the Panxi-Hannan Belt to the west of the Sichuan Basin, the occurrence of similar aged igneous rocks beneath the Sichuan Basin and with the formation of two failed rifts (the Nanhua basin to the SE of the Sichuan Basin and Kangdian basin to the west) dated between 820-760 Ma (Wang & Li, 2003) suggest that heating of the lithosphere occurred some ~125 Ma before the earliest

Ediacaran sediments were deposited in the basin. Were the source of this heat to be associated with ponding of buoyant plume material, beneath thinned lithosphere, such as proposed by the models of Sleep (2009, 2018) for the Michigan Basin then thermal cooling might be the cause of the subsidence seen in the early stages of the Sichuan Basin. The ponding of plume material would cause uplift followed by rapid subsidence. The draining away of plume material, or thermal equilibration by convection within the lowermost lithosphere, would then be followed by slow thermal subsidence. Significant km-scale uplift seems likely to have occurred in the ~125 Ma between cessation of igneous activity and deposition of the Ediacaran strata within the Sichuan Basin, because granites dated to ~800-760 Ma have been encountered in wells that have penetrated basement under the basin. However, the recent tectonic models that favour a position of South China away from the centre of Rodinia and a plume head means that there is significant uncertainty as to whether any plume material reached the Sichuan Basin area. Without further thermal modelling that might allow a prediction of the duration and amount of possible uplift with different plume scenarios it is difficult to assess whether a plume-related model might have contributed to the generation of the early subsidence in the Sichuan Basin. Such modelling is beyond the scope of the research reported here, but we suggest that it might be a fruitful avenue for further research.

Another important factor to consider is the palaeogeographic location of the Sichuan Basin in Ediacaran to Cambrian times. The majority of authors place the South China craton along the northern margin of East Gondwana, with the west Yangtze block adjacent to the proto-Tethyan ocean (Cocks & Torsvik, 2013; Zhang et al., 2015; Merdith et al., 2017; Cawood et al., 2018; Li et al., 2018). The conjugate margin is unknown, and no volcanic rocks that might indicate plume activity in the opening of Proto-Tethys are recorded at this time. On balance, the location of the Sichuan Basin adjacent to an ocean basin with subsidence increasing to the NW, in the direction of the proto-Tethyan ocean (Figure 8), does suggest that a modified lithospheric extension model, with a slow strain rate applied to thickened cratonic lithosphere, such as that proposed by Armitage and Allen (2010) might be the most applicable to explain the subsidence. Were the subsidence to be related to Rodinia plume events then we would not expect to see subsidence patterns increasing towards the location of the Ediacaran-Cambrian plate margin, but rather towards the interior of the South China craton/Yangtze block. We therefore propose that the Sichuan Basin subsidence data reported here can be interpreted as recording small amounts of pulsed extension followed by thermal cooling over a period of ~100Ma on shelfal areas and one more continuous event in deeper water areas. In this model the early Sichuan Basin would have formed a broad, ramp-like area of slow and low subsidence tilting down to the proto-Tethyan ocean located to the NW but with no major faults localizing the deformation. Without further modelling it is not possible to distinguish whether a slow-strain rate model or simpler models of instantaneous extension of 200 km thick lithosphere, may best describe the driving mechanism; or whether thermal subsidence associated with Rodinia plume activity that occurred at least 125 Myr earlier should also be considered.

6.2 Origin and evolution of the intraplatform trough

Comparing the mapped locations of the two carbonate platform margins with the contoured subsidence data allowed us to conclude that the location of the main embayed trough is not tectonically controlled. This is consistent with the lack of any mappable faults on the seismic data imaging the platform. We therefore propose that the carbonate platforms describe a palaeogeographic embayment on the shelf, with local deepening of water but that the main passive margin lay some distance to the NW in the direction of the widening of the trough and that the connection to the proto-Tethyan ocean lay to the NW. There may have been some topographic irregularities or highs on the underlying basement that controlled the location of earliest platform margin, but the resolution of the seismic data does not allow us to test this idea.

As described, the platform margins change through time, and when linked with well and core data describe a changing palaeogeography where the apex of the embayment extends southward and the entire western platform moves to the southwest at Dengying Formation Member 4 times (Figure 10b). The associated platform margins back-step and most markedly on the western side of the basin where the margin has back-stepped by up to 100 km. In the absence of a tectonic control the most likely explanation is that the movement was in response to a rise in sea level. The presence of the two karstified unconformities at the top of Members 2 and 4 of the Dengying Formation supports the interpretation of sea level control on the development of the carbonate platform. The Member 2 unconformity on the platform has long been recognized in the area and is clearly observed in numerous outcrops around the basin and in over 100 wells. Previous workers have interpreted the unconformity as forming by a crustal uplifting event related to the Tongwan movement (Li et al., 2015; Yang, Wen, Luo, Wang, & Shan, 2016; Liu et al., 2017; Zhou et al., 2017). However, the well correlations show no major erosion of Member 2, nor is there any tilting of strata or evidence of an erosional unconformity in the area as might be expected were there to have been a tectonic event affecting the area. The simplest interpretation is that a sea level fall at end Member 2 times was responsible for the emergence and karstification of the carbonate platform. Additionally, the presence of fine-grained clastic material interbedded with carbonates in thin Member 3 deposits on the platform and in the trough indicates that at times clastic material was reaching the basin, which would be consistent with rejuvenation of the hinterland, with an associated relative lowering of sea level and /or a change to a more humid climate and a switch off of carbonate production.

7 CONCLUSIONS

By Integrating seismic and well data in the central and western Sichuan Basin, we identify two phases of carbonate platform margin formation that fringed a NW-SE trending open water trough infilled with slope facies that developed in the Sichuan Basin during the Ediacaran period. The older platform margin, formed of microbial reefal mounds with carbonate shoals which formed during Member 2 of the Dengying Formation, lay out board of an open water carbonate platform with isolated reefal mounds, shoals and lagoonal deposits. At its widest in the north west of the area the trough reached a width of almost 200 km, narrowing to ~40 km in the SE. During Member 4 times a very similar paleoenvironment existed but the platform margin changed shape and back-stepped significantly, by up to 40 km on the eastern margin, and 100 km on the western margin, fringing a much wider slope area. The lack of any tectonic control on the location and shape of the platform margin, including the lack of any extensional faults visible in seismic data leads us to conclude that the Upper Ediacaran carbonate platforms describe palaeogeographic embayments on the shelf, with local deepening of water but that any deeper water basin area and ocean would have been located some distance to the NW in the direction of the widening of the trough. We propose that a rise in sea level at the end of Member 3 times or a change to a more humid climate and a switch off of carbonate production led to the widespread backstepping of the platform margin.

Contoured, backstripped, water-loaded tectonic subsidence calculated for 18 locations documents the total subsidence gradually increasing from ~400 m on the east and the southeast of the basin to over 1000 m in the NW from the Upper Ediacaran to the Lower Cambrian. Shape of subsidence curves for ~100 Ma time period from the Ediacaran to the end most closely follow theoretical subsidence curves for either instantaneous stretching or low finite strain rate (10^{-15} s^{-1}) lithospheric stretching modelled for cratonic areas with thickened lithosphere and crust. However, without further modelling we cannot discount the possibility that earlier thermal affects related to igneous plume activity between 820-760 Ma, may have played some role. In detail, the majority of wells in shelfal locations have two closely spaced events of more rapid very short subsidence events separated by ~20 Ma. The amount of lithospheric extension was low with a stretching factor of ~1.2 but increases in the NW part of the study area where it reaches 1.3-1.4. A trend of increasing subsidence to the West and North is consistent with large-scale plate reconstructions that propose that the proto-Tethyan ocean lay to the NW of the South China craton in Upper Ediacaran-Cambrian times and that the shelfal embayment opened in this direction.

We conclude that the Ediacaran carbonate platform with its NW-SW-trending trough was a palaeogeographic embayment in a large carbonate platform that covered the eastern and central parts of the present-day Sichuan Basin. The carbonate platform developed in a broad, ramp-like area of slow and low subsidence tilting down to the proto-Tethyan ocean located to the NW.

ACKNOWLEDGEMENTS

The authors thank Carl Jacquemyn, Mike Mayall, Anthony B. Watts, Nicky White, Michele Paulatto, and Alexander C. Whittaker for very helpful discussions on various aspects of this research. We especially thank Anthony B. Watts for comments on an early draft of the manuscript. Valuable comments from an anonymous reviewer, journal reviewers John Armitage, Norm Sleep and the editor Craig Magee that helped improve the manuscript are gratefully acknowledged. A university software grant from Halliburton-Landmark for seismic interpretation work conducted while Zhidong Gu was in Imperial College London supported the research. Susan Peneycad corrected the English in a first draft of this paper. This study was supported by the joint research of the RIPED of PetroChina and Imperial College London (Grant no.17HT10500000004), the Fundamental Research Project of the RIPED of PetroChina (no. 2016ycq06), and the National Petroleum Project of China (no. 2016ZX05004005-001). We thank RIPED and PetroChina for permission to publish this work.

CRediT authorship contribution statement

Zhidong Gu: Conceptualization; Formal analysis (seismic analysis, subsidence, data integration), Writing - original draft.

Lidia Lonergan: Conceptualization, Methodology, Formal analysis (subsidence), Writing - review & editing, Supervision.

Xiufen Zhai: Formal analysis (well correlation, field outcrops).

Baomin Zhang: Formal analysis (palaeogeography, field outcrops).

Weihua Lu: Formal analysis (seismic interpretation).

REFERENCES

Adams, E. W., Schroder, S., Grotzinger, J. P., & McCormick, A. S. (2004). Digital reconstruction and stratigraphic evolution of a microbial-dominated, isolated carbonate platform (Terminal Proterozoic, Nama Group, Namibia). Journal of Sedimentary Research, 74, 479-497.

Allen, P. A., & Allen, J. R. (2013). *Basin analysis: Principles and application to petroleum play assessment (third edition)*. Oxford, UK: Wiley-Blackwell.

Allen, P. A. & Armitage, J. J. (2012). Cratonic basins. In Busby, C., & Azor, A. (Eds.), *Tectonics of sedimentary basins: Recent advances* (pp. 602-620). Oxford, UK: Wiley-Blackwell.Armitage, J. J., & Allen, P. A. (2010). Cratonic basins and the long-term subsidence history of continental interiors. *Journal of the Geological Society, London*, *167*, 61-70. doi: 10.1144/0016-76492009-108

Athy, L. F. (1930). Density, porosity and compaction of sedimentary rocks. AAPG Bulletin, 14, 1-24.

Audet, D. M., & McConnell, J. D. C. (1992). Forward modelling of porosity and pore pressure evolution in sedimentary basins. *Basin Research*, *4*, 147-162.

Bally, A. W., Chou, I.-M., Clayton, R., Eugster, H. P., Kidwell, S., Meckel, L. D., …Wilson, A. A. (1986). *Notes on sedimentary basins in China*. Report of the American Sedimentary Basins Delegation to the People's Republic of China. Department of the Interior U. S. Geological Survey.

Barton, P., & Wood, R. (1984). Tectonic evolution of the North Sea basin: crustal stretching and subsidence. *Geophysical Journal of the Royal Astronomical Society*, *79*, 987-1022.

Beaumont, C., Keen, C. E., & Boutilier, R. (1982). On the evolution of rifted continental margins: comparison of models and observations for the Nova Scotian margin. *Geophysical Journal of the Royal Astronomical Society*, *70*, 667-715.

Berra, F., & Carminati, E. (2010). Subsidence history from a backstripping analysis of the Permo-Mesozoic succession of the Central Southern Alps (Northern Italy). *Basin Research*, *22*, 952-975. doi: 10.1111/j.1365-2117.2009.00453.x

Bertram, G. T., & Milton, N. J. (1989). Reconstructing basin evolution from sedimentary thickness; the importance of palaeobathymetric control, with reference to the North Sea. *Basin Research*, *1*, 247-257.

Bond, G. C., & Kominz, M. A. (1984). Construction of tectonic subsidence curves for the early Paleozoic miogeocline, southern Canadian Rocky Mountains: Implications for subsidence mechanisms, age of breakup, and crustal thinning. *Geological Society of America Bulletin*, *95*, 155-173.

Braile, L. W., Hinze, W. J., Keller, G. R., Lidiak, E. G., & Sexton, J. L. (1986). Tectonic development of the New Madrid rift complex, Mississippi Embayment, North America. *Tectonophysics*, *131*, 1-21.
Burchfiel, B. C., Chen, Z. L., Liu, Y. P., & Royden, L. H. (1995). Tectonics of the Longmen Shan and adjacent regions, central China. *International Geology Review*, *37*, 661-735. https://doi.org/10.1080/00206819509465424
Burgess, P. M., Gurnis, M., & Moresi, L. (1997). Formation of sequences in the cratonic interior of North America by interaction between mantle, eustatic, and stratigraphic processes. *Geological Society of America Bulletin*, *108*, 1515-1535.
Cao, R. J., Yang, W. R., Yin, L. M., Zhang, J. M., Li, Z. P., & Zhao, W. J. (1979). The Sinian System of southwest China. In Nanjing Institute of Geology and Palaeontology, Chinese Academy of Science (Eds.), *Carbonate biostratigraphy of southwest China* (pp. 108-154). Beijing: Science Press (in Chinese).
Cawood, P. A., Wang, Y. J., Xu, Y. J., & Zhao, G. C. (2013). Locating South China in Rodinia and Gondwana: A fragment of greater India lithosphere? Geology, 41, 903-906. doi:10.1130/G34395.1
Cawood, P. A., Zhao, G. C., Yao, J. L., Wang, W., Xu, Y. J., & Wang, Y. J. (2018). Reconstructing South China in Phanerozoic and Precambrian supercontinents. *Earth-Science Reviews*, *186*, 173-194. https://doi.org/10.1016/j.earscirev.2017.06.001
Charvet, J. (2013). The Neoproterozoic-Early Paleozoic tectonic evolution of the South China Block: An overview. *Journal of Asian Earth Sciences*, *74*, 198-209. http://dx.doi.org/10.1016/j.jseaes.2013.02.015
Chen, Q., Sun, M., Long, X. P., Zhao, G. C., & Yuan, C. (2016). U-Pb ages and Hf isotopic record of zircons from the late Neoproterozoic and Silurian-Devonian sedimentary rocks of the western Yangtze Block: Implications for its tectonic evolution and continental affinity. *Gondwana Research*, *31*, 184-199. http://dx.doi.org/10.1016/ j.gr.2015.01.009
Chen, Q., Sun, M., Long, X. P., Zhao, G. C., Wang, J., Yu, Y., & Yuan, C. (2018). Provenance study for the Paleozoic sedimentary rocks from the west Yangtze Block: Constraint on possible link of South China to the Gondwana supercontinent reconstruction. *Precambrian Research*, *309*, 271-289. http://dx.doi.org/10.1016/ j.precamres.2017.01.022
Chen, S. F., Wilson, C. J. L., Luo, Z. L., & Deng, Q. D. (1994). The evolution of the Western Sichuan Foreland Basin, southwestern China. *Journal of Southeast Asian Earth Sciences*, *10*, 159-168.Chen, Z., Zhou, C. M., Meyer, M., Xiang, K., Schiffbauer, J. D., Yuan, X. L., & Xiao, S. H. (2013). Trace fossil evidence for Ediacaran bilaterian animals with complex behaviors. *Precambrian Research*, *224*, 690-701. http://dx.doi.org/10.1016/j.precamres. 2012.11.004
Chen, Z., Zhou, C. M., Xiao, S. H., Wang, W., Guan, C. G, Hua, H., & Yuan, X. L. (2014). New Ediacaran fossils preserved in marine limestone and their ecological implications. *Scientific Reports*, *4*, 4180. DOI: 10.1038/srep04180
Cocks, L. R. M. & Torsvik, T. H. (2013). The dynamic evolution of the Palaeozoic geography of eastern Asia. *Earth-Science Reviews*, *117*, 40-79. http://dx.doi.org/ 10.1016/j.earscirev.2012.12.001
Cohen, K. M., Harper, D. A. T., & Gibbard, P. L. (2018). *ICS International Chronostratigraphic Chart 2018/08*. International Commission on Stratigraphy, IUGS. www.stratigraphy.org (visited: 2018/08/17).
Condon, D., Zhu, M. Y., Bowring, S., Wang, W., Yang, A. H., & Jin, Y. G. (2005). U-Pb ages from the Neoproterozoic Doushantuo Formation, China. *Science*, *308*, 95-98. DOI: 10.1126/science.1107765
Deng, S. L., Song, J. M., Liu, S. G., Luo, P., Li, Z. W., Yang, D., … Li, L. J. (2020). Mixed sedimentary characteristics of the third Member of Dengying Formation, Sichuan Basin, and its geological significance. *Acta Sedimentologica Sinica*, *38*, 598-612 (in Chinese with English abstract). DOI: 10.14027/j.issn.1000‑0550.2019.109
Dong, Y. P., Zhang, X. N., Liu, X. M., Li, W., Chen, Q., Zhang, G. W., … Zhang, F. F. (2015). Propagation tectonics and multiple accretionary processes of the Qinling Orogen. *Journal of Asian Earth Sciences*, *104*, 84–98. http://dx.doi.org/10.1016/j.jseaes. 2014.10.007
Downey, N. K., & Gurnis, M. (2009). Instantaneous dynamics of the cratonic Congo basin. *Journal of Geophysical Research*, *114*, B06401. doi:10.1029/2008JB006066
Du, J. H., Zou, C. N., Xu, C. C., He, H. Q., Shen, P., Yang, Y. M., … Yang, Y. (2014). Theoretical and technical innovations in strategic discovery of a giant gas field in Cambrian Longwangmiao Formation of central Sichuan paleo-uplift, Sichuan Basin. *Petroleum Exploration and Development*, *41*, 294-305.
Du, J. H., Wang, Z. C., Zou, C. N., Xu, C. C., Shen, P., Zhang, B. M., … Huang, S. P. (2016). Discovery of intracratonic rift in the Upper Yangtze and its control effect on the formation of Anyue giant gas

field. *Acta Petrolei Sinica*, *37*, 1-16 (in Chinese with English abstract). DOI: 10.7623/SYXB201601001

Duda, J.-P., Zhu, M. Y., & Reitner, J. (2016). Depositional dynamics of a bituminous carbonate facies in a tectonically induced intra-platform basin: the Shibantan Member (Dengying Formation, Ediacaran Period). *Carbonates Evaporites*, *31*, 87-99. DOI 10.1007/s13146-015-0243-8

Farrington, R. J., Stegman, D. R., Moresi, L. N., Sandiford, M., & May, D. A. (2010). Interactions of 3D mantle flow and continental lithosphere near passive margins. *Tectonophysics*, *483*, 20-28. doi:10.1016/j.tecto.2009.10.008

Fowler, C. M. R., & Nisbet, E. G. (1985). The subsidence of the Williston Basin. *Canadian Journal of Earth Sciences*, *22*, 408-415.

Fu, Q. L., Hu, S. Y., Xu, Z. H., Zhao, W. Z., Shi, S. Y., & Zeng, H. L. (2020). Depositional and diagenetic controls on deeply buried Cambrian carbonate reservoirs: Longwangmiao Formation in the Moxi-Gaoshiti area, Sichuan Basin, southwestern China. *Marine and Petroleum Geology*, *117*, 104318. https://doi.org/10.1016/ j.marpetgeo. 2020.104318

Gao, R., Chen, C., Wang, H. Y., Lu, Z. W., Brown, L., Dong, S. W., … Li, F. (2016). SINOPROBE deep reflection profile reveals a Neo-Proterozoic subduction zone beneath Sichuan Basin. *Earth and Planetary Science Letters, 454*, 86-91. http://dx.doi.org/10.1016/j.epsl.2016.08.030

Giles, M. R. (1997). *Diagenesis: A quantitative perspective*. Implications for basin Mmodelling and rock property prediction (pp.526). Dordrecht, Boston, London: Kluwer Academic Publishers.

Grotzinger, J., & Al-Rawahi, Z. (2014). Depositional facies and platform architecture of microbialite-dominated carbonate reservoirs, Ediacaran–Cambrian Ara Group, Sultanate of Oman. *AAPG Bulletin*, *98*, 1453-1494. DOI: 10.1306/02271412063

Gu, Z. D., Zhang, W., & Yuan, M. (2014). Zircon SHRIMP U-Pb dating of basal granite and its geological significance in Weiyuan area of Sichuan Basin. *Chinese Journal of Geology*, *49*, 202-213 (in Chinese with English abstract).

Gu, Z. D., & Wang, Z. C. (2014). The discovery of Neoproterozoic extensional structures and its significance for gas exploration in the Central Sichuan Block, Sichuan Basin, South China. *Science China: Earth Sciences, 57*, 2758-2768. doi: 10.1007/s11430-014-4961-x

Gu, Z. D., Yin, J. F., Jiang, H., Li, Q. F., Zhai, X. F., Huang, P. H., … Zhang, H. (2016). Discovery of Xuanhan-Kaijiang paleouplift and its significance in the Sichuan Basin, SW China. *Petroleum Exploration and Development*, *43*, 976-987.

Gu, Z. D., Wang, X., Nunns, A., Zhang, B., Jiang, H., Fu, L., & Zhai, X. F. (2021). Structural styles and evolution of a thin-skinned fold-and-thrust belt with multiple detachments in the eastern Sichuan Basin, South China. *Journal of Structural Geology*, 142, 104191. https://doi.org/10.1016/j.jsg.2020.104191

Guo, Z. W., Deng, K. L., Han, Y. H., Liu, Y. K., Yin, J. T., Wang, Q. G., …Zhao, Z. H. (1996). *The formation and evolution of the Sichuan Basin*. Beijing: Geological Publishing Press (in Chinese).

Hartley, R. W., & Allen, P. A. (1994). Interior cratonic basins of Africa: relation to continental break-up and role of mantle convection. *Basin Research*, *6*, 95-113.

Jarvis, G. T., & McKenzie, D. P. (1980). Sedimentary basin formation with finite extension rates. *Earth and Planetary Science Letters*, *48*, 42-52. https://doi.org/10.1016/0012-821X(80)90168-5

Jiang, G. Q., Shi, X. Y., Zhang, S. H., Wang, Y., & Xiao, S. H. (2011). Stratigraphy and paleogeography of the Ediacaran Doushantuo Formation (ca. 635-551 Ma) in South China. *Gondwana Research*, *19*, 831-849. doi:10.1016/j.gr.2011.01.006Huang, J. Z. (1985). Geochemical characteristics of natural gases in the Sichuan basin. *Geochemistry*, *4*, 343-361.

Korsch, R. J., Mai, H. Z., Sun, Z. C, & Gorter, J. D. (1991). The Sichuan Basin, southwest China: a Late Proterozoic (Sinian) petroleum province. *Precambrian Research*, *54*, 45-63.

Lambert, I. B., Walter, M. R., Zang, W. L., Lu, S. N., & Ma, G. G. (1987). Palaeoenvironment and carbon isotope stratigraphy of Upper Proterozoic carbonates of the Yangtze Platform. *Nature*, *325*, 140-142.

Lee, E. Y., Novotny, J., & Wagreich, M. (2016). BasinVis 1.0: A MATLAB®-based program for sedimentary basin subsidence analysis and visualization. Computers & Geosciences, 91, 119-217. http://dx.doi.org/10.1016/j.cageo.2016.03.013

Le Pichon, X., & Sibuet, J.-C. (1981). Passive margins: A model of formation. *Journal of Geophysical research*, *86*, 3708-3720.

Li, J. Y., Wang, X. L., & Gu, Z. D. (2018). Early Neoproterozoic arc magmatism of the Tongmuliang Group on the northwestern margin of the Yangtze Block: Implications for Rodinia Assembly. *Precambrian Research*, *309*, 181-197, http://dx.doi.org/10.1016/ j.precamres.2017.04.040

Li, L., Tan, X. C., Zeng, W., Zhou, T., Yang, Y., Hong, H. T., … Bian, L. Z. (2013). Development and reservoir significance of mud mounds in Sinian Dengying Formation, Sichuan Basin. *Petroleum Exploration Development*, *40*, 714-721.

Li, S. Z., Zhao, S. J., Liu, X., Cao, H. H., Yu, S., Li, X. Y., … Suo, Y. H. (2018). Closure of the Proto-Tethys Ocean and Early Paleozoic amalgamation of microcontinental blocks in East Asia. *Earth-Science Reviews, 186*, 37-75. http://dx.doi.org/10.1016/ j.earscirev.2017.01.011

Li, W., Yu, H. Q., & Deng, H. B. (2012). Stratigraphic division and correlation and sedimentary characteristics of the Cambrian in central-southern Sichuan Basin. *Petroleum Exploration and Development*, *39*, 725-735.

Li, Z. X., Li, X. H., Kinny, P. D., & Wang, J. (1999). The breakup of Rodinia: did it started with a mantle plume beneath South China? *Earth and Planetary Science Letters, 173*, 171-181. DOI:10.1016/s0012-821x(99)00240-x

Li, Z. X., Li, X. H., Kinny, P. D., Wang, J., Zhang, S., & Zhou, H. (2003). Geochronology of Neoproterozoic syn-rift magmatism in the Yangtze Craton, South China and correlations with other continents: evidence for a mantle superplume that broke up Rodinia. *Precambrian Research*, *122*, 85-109.

Li, Z. Q., Liu, J., Li, Y., Hang, W. Y., Hong, H. T., Ying, D. L., … Peng, J. (2015). Formation and evolution of Weiyuan-Anyue tensional corrosion trough in Sinian system, Sichuan Basin. *Petroleum Exploration and Development, 42*, 29-36.

Lin, X. X, Peng, J., Du, L. C., Yan, J. P., & Hou, Z. J. (2017). Characterization of the microbial dolomite of the Upper Sinian Dengying Formation in the Hanyuan area of Sichuan Province, China. *Acta Geologica Sinica (English Edition)*, *91*, 806-821.

Liu, H. S. (1979). Mantle convection and subcrustal stresses under Australia. *Modern Geology*, *7*, 29-36.

Liu, P. J., Chen, S. M., Zhu, M. Y., Li, M., Yin, C. Y, & Shang, X. D. (2014). High-resolution biostratigraphic and chemostratigraphic data from the Chenjiayuanzi section of the Doushantuo Formation in the Yangtze Gorges area, South China: Implication for subdivision and global correlation of the Ediacaran System. *Precambrian Research*, *249*, 199-214. http://dx.doi.org/10.1016/j.precamres.2014.05.014

Liu, J. J., Li, W., Zhang, B. M., Zhou, H., Yuan, X. H., Shan, X. Q., Zhang, J., … Li, X. (2015). Sedimentary palaeogeography of the Sinian in Upper Yangtze region. *Journal of Palaeogeography*, *17*, 735-753 (in Chinese with English abstract).

Liu, S., Ning, M., & Xie, G. P. (2015). Geological significance of paleo-aulacogen and exploration potential of reef flat gas reservoirs in the Western Sichuan Depression. Natural Gas Industry, B2, 406-414. http://dx.doi.org/10.1016/j.ngib.2015.09.016

Liu, S. G., Deng, B., Jansa, L., Zhong, Y., Sun, W., Song, J. M., … Tian, Y. H. (2017). The Early Cambrian Mianyang-Changning intracratonic sag and its control on petroleum accumulation in the Sichuan Basin, China. Geofluids, 1-16. https://doi.org/ 10.1155/2017/6740892

Luo, B., Yang, Y., Zhou, G., Luo, W. J., Shan, S. J., & Xia, M. L. (2018). Basic characteristics and accumulation mechanism of Sinian-Cambrian giant highly mature and oil-cracking gas reservoirs in the Sichuan Basin, SW China. *Energy Exploration & Exploitation*, *36*, 568-590. DOI: 10.1177/0144598717736856

McKenzie, D. (1978). Some remarks on the development of sedimentary basins. *Earth and Planetary Science Letters*, *40*, 25-32.

McKenzie, D., & Priestley, K. (2016). Speculations on the formation of cratons and cratonic basins. *Earth and Planetary Science Letters*, *435*, 94-104. http://dx.doi.org/10.1016/j.epsl.2015.12.010

McKenzie, D., & Tribaldos, V. R. (2018). Lithospheric heating by crustal thickening: a possible origin of the Parnaíba Basin. In Daly, M. C., Fuck, R. A., Julia, J., Macdonald, D. I. M., & Watts, A. B. (Eds.), *Cratonic basin formation: a case study of the Parnaíba Basin of Brazil*. Geological Society, London, Special Publications, 472, 37-44. https://doi.org/10.1144/SP472.5

Meng, Q. R., Zhang, G. W., Yu, Z. P., & Mei, Z. C. (1996). Late Paleozoic sedimentation and tectonics of rift and limited ocean basin at southern margin of the Qinling. *Science in China (Series D)*, *39 (Supp.)*, 24-32.

Merdith, A. S, Collins, A. S., Williams, S. E., Pisarevsky, S., Foden, J. D., Archibald, D. B., ... Müller, R. D. (2017). A full-plate global reconstruction of the Neoproterozoic. *Gondwana Research*, *50*, 84-134. http://dx.doi.org/10.1016/j.gr.2017.04.001

Nunn, J. A., & Sleep, N. H. (1984). Thermal contraction and flexure of intracratonal basins: a three-dimensional study of the Michigan basin. *Geophysical Journal of the Royal Astronomical Society*, *76*, 587-635.

Peng, S., Babcock, L. E., & Cooper, R. A. (2012). The Cambrian Period. In Gradstein, F. M., Ogg, J. G., Schmitz, M. D., & Ogg, G. M. (Eds), *The Geologic Time Scale 2012* (pp. 437-488). Elsevier B. V. DOI: 10.1016/B978-0-444-59425-9.00019-6.

Priestley, K., & McKenzie, D. (2013). The relationship between shear wave velocity, temperature, attenuation and viscosity in the shallow part of the mantle. *Earth and Planetary Science Letters*, *381*, 78-91. https://doi.org/10.1016/j.epsl.2013.08.022Quinlan, G. M. (1987). Models of subsidence mechanisms in intracratonic basins and their applicability to North American examples. In Beaumont, C., & Tankard, A. J. (Eds.), *Sedimentary basins and basin-forming mechanisms* (pp. 463-481). Memoir Canadian Society Petroleum Geologists 12.

Ren, Y., Zhong, D. K., Gao, C. L., Yang, Q. Q., Xie, R., Jia, L. B., … Zhong, N. C. (2017). Dolomite geochemistry of the Cambrian Longwangmiao Formation, eastern Sichuan Basin: Implication for dolomitization and reservoir prediction. *Petroleum Research*, *2*, 64-76. http://dx.doi.org/10.1016/j.ptlrs.2017.06.002

Richardson, N. J., Densmore, A. L., Seward, D., Fowler, A., Wipf, M., Ellis, M. A., … Zhang, Y. (2008). Extraordinary denudation in the Sichuan Basin: Insights from low-temperature thermochronology adjacent to the eastern margin of the Tibetan Plateau. *Journal of Geophysical Research*, *113*, B04409. doi:10.1029/2006JB004739

Schmoker, J. W., & Halley, R. B. (1982). Carbonate porosity versus depth: A predictable relation for South Florida. *AAPG Bulletin*, *66*, 2561-2570.

Sclater, J. G., & Christie, P. A. F. (1980). Continental stretching: An explanation of the post-mid-Cretaceous subsidence of the central North Sea Basin. *Journal of Geophysical Research*, *85*, 3711-3739.

Shen, A. J., Hu, A. P., Pan, L. Y., & She, M. (2017). Origin and distribution of grain dolostone reservoirs in the Cambrian Longwangmiao Formation, Sichuan Basin, China. *Acta Geologica Sinica (English Edition)*, *91*, 204-218.

Sleep, N. H. (2009). Stagnant lid convection and the thermal subsidence of sedimentary basins with reference to Michigan. *Geochemistry, Geophysics, Geosystems*, *10*, Q12015. https://doi.org/10.1029/2009GC002881

Sleep, N. H. (2018). Cratonic basins with reference to the Michigan basin. In Daly, M. C., Fuck, R. A., Julià, J., Macdonald, D. I. M., & Watts, A. B. (Eds.), *Cratonic basin formation: a case study of the Parnaíba Basin of Brazil*. Geological Society, London, Special Publications, 472, 17-35. https://doi.org/10.1144/SP472.1

Sloss, L. L. (1963). Sequences in the cratonic interior of North America. *Geological Society of America Bulletin*, *74*, 93-114.

Sloss, L. L., & Speed, R. C. (1974). Relationships of cratonic and continental-margin tectonic episodes. *Paleontologists and Mineralogists*, *22*, 98-119.

Song, J. M., Liu, S. G., Qing, H. R., Jansa, L., Li, Z. W., Luo, P., … Lin, T. (2018). The depositional evolution, reservoir characteristics, and controlling factors of microbial carbonates of Dengying Formation in upper Neoprotozoic, Sichuan Basin, Southwest China. *Energy Exploration & Exploitation*, *36*, 591-619. DOI: 10.1177/ 0144598717743995.

Steckler, M. S., & Watts, A. B. (1978). Subsidence of the Atlantic-type continental margin off New York. *Earth and Planetary Science Letters*, *41*, 1-13.

Stecker, M. S., & Watts, A. B. (1981). Subsidence history and tectonic evolution of Atlantic-type continental margins. In Scrutton, R. A. (Eds.), *Dynamics of passive margins, Geodynamics, Volume 6* (pp. 184-196). Washington, DC: American Geophysical Union.

Torsvik, T. H., & Cocks, L. R. M. (2017). *Earth history and palaeogeography*. Cambridge, UK: Cambridge University Press, pp. 317.

Tozer, B., Watts, A. B., & Daly, M. C. (2017). Crustal structure, gravity anomalies, and subsidence history of the Parnaíba cratonic basin, Northeast Brazil. *Journal of Geophysical Research: Solid Earth*, *122*, 5591–5621. doi:10.1002/2017JB014348

Vernhet, E., & Reijmer, J. J. G. (2010). Sedimentary evolution of the Ediacaran Yangtze platform shelf (Hubei and Hunan provinces, Central China). Sedimentary Geology, 225, 99-115.

Vyssotski, A. V., Vyssotski, V. N., & Nezhdanov, A. A. (2006). Evolution of the West Siberian Basin. *Marine and Petroleum Geology*, *23*, 93-126. doi:10.1016/j.marpetgeo.2005.03.002

Wang, J., & Li, Z. X. (2003). History of Neoproterozoic rift basins in South China: implications for Rodinia break-up. *Precambrian Research*, *122*, 141-158.

Wang, Y. J., Zhang, Y. H., Fan, W. M., & Peng, T. P. (2005). Structural signatures and $^{40}Ar/^{39}Ar$ geochronology of the Indosinian Xuefengshan tectonic belt, South China Block. *Journal of Structural Geology*, *27*, 985-998. doi:10.1016/j.jsg.2005.04.004

Wang, Z. C., Jiang, H., Wang, T. S., Lu, W. H., Gu, Z. D., Xu, A. N., … Xu, Z. H. (2014). Paleo-geomorphology formed during Tongwan tectonization in Sichuan Basin and its significance for hydrocarbon accumulation. *Petroleum Exploration and Development*, *41*, 338-345.

Wang, W., Cawood, P. A., Pandit, M. K., Xia, X. P., Raveggi, M., Zhao, J. H., …Qi, L. (2021). Fragmentation of South China from greater India during the Rodinia-Gondwana transition. *Geology, 49*, 228-232. https://doi.org/10.1130/G48308.1

Watts, A. B., & Steckler, M. S. (1979). Subsidence and eustasy at the continental margin of eastern North America. In Deep Drilling Results in the Atlantic Ocean: Continental margins and paleoenvironment, *Maurice Ewing Series*, *Volume 3* (pp. 218-234), American Geophysical Union.

Watts, A. B. (1982). Tectonic subsidence, flexure and global changes of sea level. *Nature*, *297*, 469-474.

Watts, A. B., Tozer, B., Daly, M. C., & Smith, J. (2018). A comparative study of the Parnaíba, Michigan and Congo cratonic basins. In Daly, M. C., Fuck, R. A., Julià, J., Macdonald, D. I. M., & Watts, A. B. (Eds.), *Cratonic basin formation: a case study of the Parnaíba Basin of Brazil*. Geological Society, London, Special Publications, 472, 45-66. https://doi.org/10.1144/SP472.6

Wei, G. Q., Yang, W., Du, J. H., Xu, C. C., Zou, C. N., Xie, W. R., … Wu, S. J. (2015). Geological features of Sinian-Early Cambrian intracratonic rift of the Sichuan Basin. *Natural Gas Industry*, *B2*, 37-48. http://dx.doi.org/10.1016/j.ngib.2015.02.004

Xie, X. Y., & Heller, P. L. (2009). Plate tectonics and basin subsidence history. Geological Society of America Bulletin, 121, 55–64. doi: 10.1130/B26398.1

Xu, Y. J., Cawood, P. A., Du, Y. S., Hu, L. S., Yu, W. C., Zhu, Y. H., & Li, W. C. (2013). Linking south China to northern Australia and India on the margin of Gondwana: Constraints from detrital zircon U-Pb and Hf isotopes in Cambrian strata. *Tectonics*, *32*, 1547-1558. doi:10.1002/tect.20099

Yan, D. P., Zhou, Y., Qiu, L., Wells, M. L., Mu, H. X., & Xu, C. G. (2018). The Longmenshan tectonic complex and adjacent tectonic units in the eastern margin of the Tibetan Plateau: A review. *Journal of Asian Earth Sciences*, *164*, 33–57. https://doi.org/10.1016/j.jseaes.2018.06.017

Yang, C., Li, X. H., Zhu, M. Y., & Condon, D. J. (2017). SIMS U-Pb zircon geochronological constraints on upper Ediacaran stratigraphic correlations, South China. *Geological Magazine*, *154*, 1202-1216. doi:10.1017/S0016756816001102

Yang, Y. M., Wen, L., Luo, B., Wang, W. Z., & Shan, S. J. (2016). Hydrocarbon accumulation of Sinian natural gas reservoirs, Leshan-Longnüsi paleohigh, Sichuan Basin, SW China. Petroleum Exploration and Development, 43, 197-207.

Yong, L., Allen, P. A., Densmore, A. L., & Qiang, X. (2003). Evolution of the Longmen Shan foreland basin (western Sichuan, China) during the Late Triassic Indosinian Orogeny. *Basin Research*, *15*, 117-138.

Zhai, X. F., Luo, P., Gu, Z. D., Jiang, H., Zhang, B. M., Wang, Z. C., … Wu, S. T. Microbial mineralization of botryoidal laminations in the Upper Ediacaran dolostones, Western Yangtze Platform, SW China. Journal of Asian Earth Sciences, 195, 104334. https://doi.org/10.1016/j.jseaes.2020.104334

Zhang, W. T, Yuan, K. X, Zhou, Z. Y., Qian, Y., & Wang, Z. Z. (1979). The Cambrian System of southwest China. In Nanjing Institute of Geology and Palaeontology, Chinese Academy of Science (Eds.), *Carbonate biostratigraphy of southwest China* (pp. 39-107). Beijing: Science Press (in Chinese).

Zhang, S. H., Jiang, G. Q., Zhang, J. M., Song, B., Kennedy, M. J., & Christie-Blick, N. (2005). U-Pb sensitive high-resolution ion microprobe ages from the Doushantuo Formation in south China: Constraints on late Neoproterozoic glaciations. *Geology*, *33*, 473-476. doi: 10.1130/G21418.1

Zhang, S. H., Evans, D. A. D., Li, H. Y., Wu, H. C, Jiang, G. Q., Dong, J., … Yang, T. S. (2013). Paleomagnetism of the late Cryogenian Nantuo Formation and paleogeographic implications for the South China Block. *Journal of Asian Earth Sciences*, *72*, 164-177. http://dx.doi.org/10.1016/j.jseaes.2012.11.022

Zhang, S. H., Li, H. Y., Jiang, G. Q., Evans, D. A. D., Dong, J., Wu, H. C., … Xiao, Q. S. (2015). New paleomagnetic results from the Ediacaran Doushantuo Formation in South China and their paleogeographic implications. *Precambrian Research*, *259*, 130-142. http://dx.doi.org/10.1016/j.precamres.2014.09.018

Zhao, G. C., & Cawood, P. A. (2012). Precambrian geology of China. *Precambrian Research*, *222-223*, 13-54. http://dx.doi.org/10.1016/j.precamres.2012.09.017

Zhao, J. H., Li, Q. W., Liu, H., & Wang, W. (2018). Neoproterozoic magmatism in the western and northern margins of the Yangtze Block (South China) controlled by slab subduction and subduction-transform-edge-propagator. *Earth-Science Reviews*, *187*, 1-18. https://doi.org/10.1016/j.earscirev.2018.10.004

Zhou, Z., Wang, X. Z., Yin, G., Yuan, S. S., & Zeng, S. J. (2016). Characteristics and genesis of the (Sinian) Dengying Formation reservoir in Central Sichuan, China. *Journal of Natural Gas Science and Engineering*, *29*, 311-321. http://dx.doi.org/10.1016/ j.jngse.2015.12.005

Zhou, H., Li, W., Zhang, B. M., Liu, J. J., Deng, S. H., Zhang, S. B., … Jiang, H. (2017). Formation and evolution of intraplatform basin from the late Sinian to early Cambrian in Sichuan Basin, China. *Petroleum Research*, *2*, 41-53. http://dx.doi.org/10.1016/ j.ptlrs.2017.01.001

Zhou, C. M, Yuan, X. L, Xiao, S. H, Chen, Z., & Hua, H. (2019). Ediacaran integrative stratigraphy and timescale of China. *Science China Earth Sciences*, *62*, 7-24. https://doi.org/10.1007/s11430-017-9216-2

Zhu, M. Y., Zhang, J. M., Steiner, M., Yang, A. H., Li, G. X., & Erdtmann, B. D. (2003). Sinian-Cambrian stratigraphic framework for shallow- to deep-water environments of the Yangtze Platform: an integrated approach. *Progress in Natural Science*, *13*, 951-960.

Zhu, M. Y., Zhang, J. M., & Yang, A. H. (2007). Integrated Ediacaran (Sinian) chronostratigraphy of South China. *Palaeogeography, Palaeoclimatology, Palaeoecology*, *254*, 7-61. doi:10.1016/j.palaeo.2007.03.025

Zhu, G. Y., Wang, T. S., Xie, Z. Y., Xie, B. H., & Liu, K. Y. (2015). Giant gas discovery in the Precambrian deeply buried reservoirs in the Sichuan Basin, China: Implications for gas exploration in old cratonic basins. *Precambrian Research*, *262*, 45-66. https://doi.org/10.1016/j.precamres.2015.02.023

Zou, C. N., Du, J. H., Xu, C. C., Wang, Z. C., Zhang, B. M., Wei, G. Q., …Gu, Z. D. (2014). Formation, distribution, resource potential, and discovery of Sinian-Cambrian giant gas field, Sichuan Basin, SW China. *Petroleum Exploration and Development*, *41*, 306-325.

FIGURE CAPTIONS

FIGURE 1 (a) Topographic map of Sichuan Basin and surrounding areas illustrating the regional tectonic setting. The Sichuan Basin is located within the South China Craton (inset map). (b) Simplified stratigraphy of the Sichuan Basin, which consists of two sedimentary megasequences: a carbonate-dominated marine succession from Ediacaran to Middle Triassic and clastic, terrestrial rocks from the Upper Triassic to Quaternary. (c) Simplified cross section across the Sichuan Basin from the Longmenshan Fold-thrust Belt in the NW, to the eastern Sichuan Fold-thrust Belt in the SE. Section is located by black line in (a). Modified from Gu et al. (2021).

FIGURE 2 Geological map of the western and central Sichuan Basin and surrounding mountain belts; modified from Yan et al. (2018). Black lines are the location of seismic sections A-E in Figures 4-7; circles are location of wells used in the paper, including six pseudo wells, PS1-PS6. The solid blue lines are the mapped locations of Upper Ediacaran platform margins interpreted from seismic and well data. The dashed blue line is the back-stepped position of the youngest platform margin based on well interpretation, and outcrop data.

FIGURE 3 Stratigraphy of Ediacaran to Lower Cambrian rocks in the Sichuan Basin, illustrating variation in thickness and lithology across the carbonate platforms and trough. The seismic expression of the mapped stratigraphic events is shown in column on the right. The Ediacaran System (Sinian in Chinese literature) consists of the Doushantuo Formation of the Lower Ediacaran and the Dengying Formation of the Upper Ediacaran. The Dengying Formation comprises four members, Member 1 to Member 4 (Z_2dn^1-Z_2dn^4 in Chinese literature). The Lower Cambrian consists of the Maidiping, Qiongzhusi, Canglangpu, and Longwangmiao Formations. The Dengying Formation thins from the platform margins to the trough, while the Lower Cambrian thickens within the trough.

FIGURE 4 Seismic section A across the northern part of the intraplatform trough (location shown on Figure 2); uninterpreted (a) and interpreted (b). The sections show the thinning of the Dengying Formation to the NW (blue Members 1-2 of Upper Ediacaran), the development of the two platform margins, the filling of the trough and onlapping of the platform margin by the Lower Cambrian. Note the distance over which the Member 4 platform margin has back-stepped.

FIGURE 5 Seismic sections illustrating detail of the older (a) and younger (b) platform margins from seismic line A; location shown in Figure 4a. Data are shown at approximately a 1:1 scale. Section (a) images the first platform margin; the disrupted reflections are interpreted as talus deposits; onlap of the Lower Cambrian is evident. Section (b) shows the second platform margin and onlap of the Lower Cambrian in more detail.

FIGURE 6 Seismic sections B, C, D, perpendicular to the trough margin in the centre of study area. Sections are located on Figure 2. All three sections image both platform margins, and onlap of the Lower Cambrian. Potential clinoforms associated with the younger platform margin are visible in Section C (arrowed). The fourth section is a detail of the youngest platform margin (arrowed). Note the lensoid body associated with the platform build-up.

FIGURE 7 Seismic section E from a 3-D dataset located on western margin of the trough, showing the older platform margin, with Cambrian strata onlapping the relief associated with the platform edge. The seismic line is located is on Figure 2.

FIGURE 8 Isopach maps of the Upper Ediacaran to Lower Cambrian. (a) Isopach map of all members of the Dengying Formation which shows a NW-SE oriented low widening to the N, with thick carbonate platform margins on the E and W flanks of the trough. (b) Members 1 and 2 isopach map. The thickness change from the platform margin to the trough allows the margins of the oldest platform to be clearly located. (c) Member 4 isopach map shows the location of the younger platform margin on the E side of the trough. (d) The isopach map of the Lower Cambrian shows the main Early Cambrian depocentre as the sediments infilled the trough. Solid circles are sites of the wells used in the paper, including six pseudo wells PS1-PS6. Black line in Figure 8(a) is the location of the well correlation shown in Figure 9.

FIGURE 9 Well correlation for the Upper Ediacaran to Lower Cambrian units from SW (left) to NE (right) across the intraplatform trough (see Figure 8 for location). Note the considerable thickness variations of the Dengying Formation (Z_2dn^{1-2}, Z_2dn^4) and Lower Cambrian ($Є_1m$- $Є_1q$) across the trough and adjacent platforms.

FIGURE 10 (a) Palaeogeography of Member 2 of the Dengying Formation (Z_2dn^2) based on the interpretation of seismic data, well logs and cores. Microbial mounds and shoals are abundant on the platform margins forming long narrow belts. (b) Palaeogeography of Member 4 of the Dengying Formation (Z_2dn^4) based on the interpretation of seismic data, well logs and cores. The black line is the locations of the well correlation in Figure 9.

FIGURE 11 Subsidence curves of well GS1 in the centre of the basin illustrating the main basin forming events in the Sichuan Basin. Blue line is the decompacted subsidence; red line is the backstripped water-loaded subsidence. Data in Richardson et al. (2008) was used to give a semi quantitative estimate of what the maximum foreland basin subsidence might have been assuming 4 km of erosion of late Jurassic to Tertiary sediments in the last 40 Ma.

FIGURE 12 Decompacted subsidence curves (blue lines) and backstripped water-loaded tectonic subsidence curves (red lines) for 18 wells/pseudo wells in the basin; wells are located in Figure 2. The subsidence curves in many of the wells are affected by later tectonic movement during the Late Ordovician to Silurian causing considerable uplift and erosion, such as ZY1, Z4, HS1, LT1, and PS1 to PS6; missing sections are shown by dashed lines.

FIGURE 13 Contours of the cumulative tectonic subsidence in kilometers during the Ediacaran to Early Cambrian. (a) Early Ediacaran (equivalent to the Doushantuo Formation); (b) early Late Ediacaran (equivalent to Z_2dn^{1-2}); (c) late Late Ediacaran (equivalent to Z_2dn^4); (d) Early Cambrian (equivalent to the Maidiping and Qiongzhushi Formations). The platform margins (in blue) are shown for reference. Note in Early Cambrian times (d) the trough was being infilled and the carbonate platform was no longer active. The solid line is the location of the cross section in Figure 14.

FIGURE 14 2-D reconstruction of backstripped tectonic subsidence from the Ediacaran to Early Cambrian calculated from subsidence contours (Section located in Figure 13). Note lack of correlation between increased gradient in subsidence at Dengying Formation times (Between red lines) and location of the platform margins. (a) Early Ediacaran (equivalent to the Doushantuo Formation); (b) early Late Ediacaran (equivalent to Z_2dn^{1-2}); (3) late Late Ediacaran (equivalent to Z_2dn^4); (4) Early Cambrian (equivalent to the Maidiping and Qiongzhushi Formations, $Є_1m$- $Є_1q$).

FIGURE 15 Comparison of calculated water-loaded subsidence for six locations in the Sichuan Basin (coloured lines) with theoretical models from Armitage and Allen (2010). The grey lines are for a model of instantaneous extension; dashed lines for finite extension at a slow strain rate of $10^{-15}s^{-1}$. The theoretical models have a 200 km thick lithosphere, and a 40 km thick crust. The amount of lithospheric extension for instantaneous extension was low with a stretching factor of ~1.2 (wells LL1, GS17, MS1, and HT1), but increases in the NW part of the study area where it reaches 1.3-1.4 (wells LT1 and PS6).

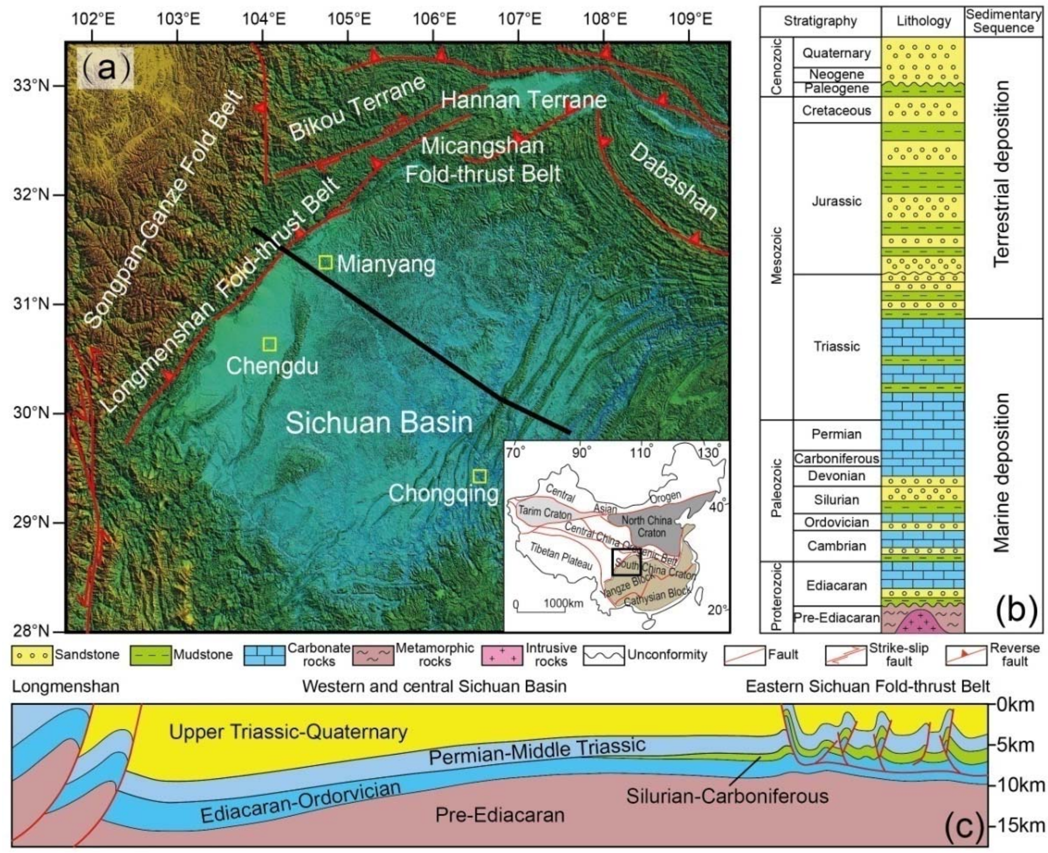

FIGURE 1 (a) Topographic map of Sichuan Basin and surrounding areas illustrating the regional tectonic setting. The Sichuan Basin is located within the South China Craton (inset map). (b) Simplified stratigraphy of the Sichuan Basin, which consists of two sedimentary megasequences: a carbonate-dominated marine succession from Ediacaran to Middle Triassic and clastic, terrestrial rocks from the Upper Triassic to Quaternary. (c) Simplified cross section across the Sichuan Basin from the Longmenshan Fold-thrust Belt in the NW, to the eastern Sichuan Fold-thrust Belt in the SE. Section is located by black line in (a). Modified from Gu et al. (2021).

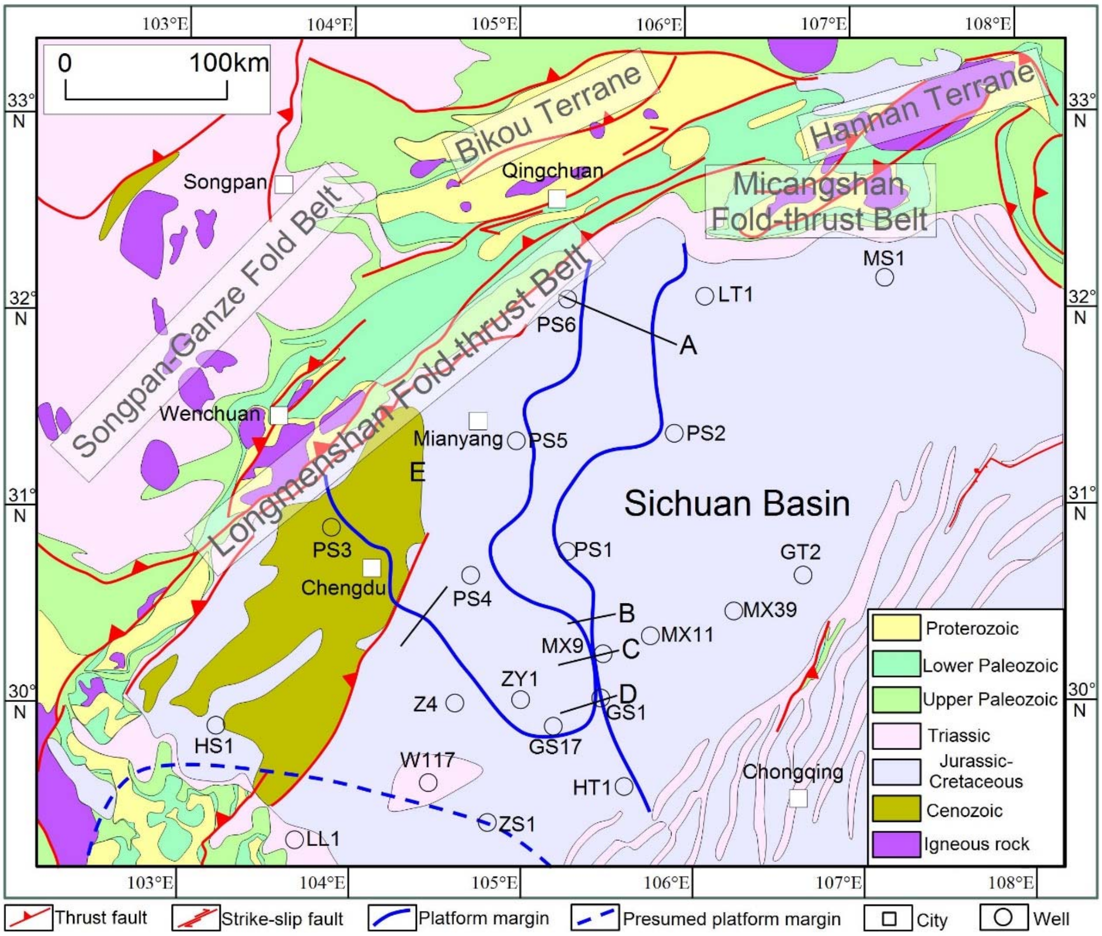

FIGURE 2 Geological map of the western and central Sichuan Basin and surrounding mountain belts; modified from Yan et al. (2018). Black lines are the location of seismic sections A-E in Figures 4-7; circles are location of wells used in the paper, including six pseudo wells, PS1-PS6. The solid blue lines are the mapped locations of Upper Ediacaran platform margins interpreted from seismic and well data. The dashed blue line is the back-stepped position of the youngest platform margin based on well interpretation, and outcrop data.

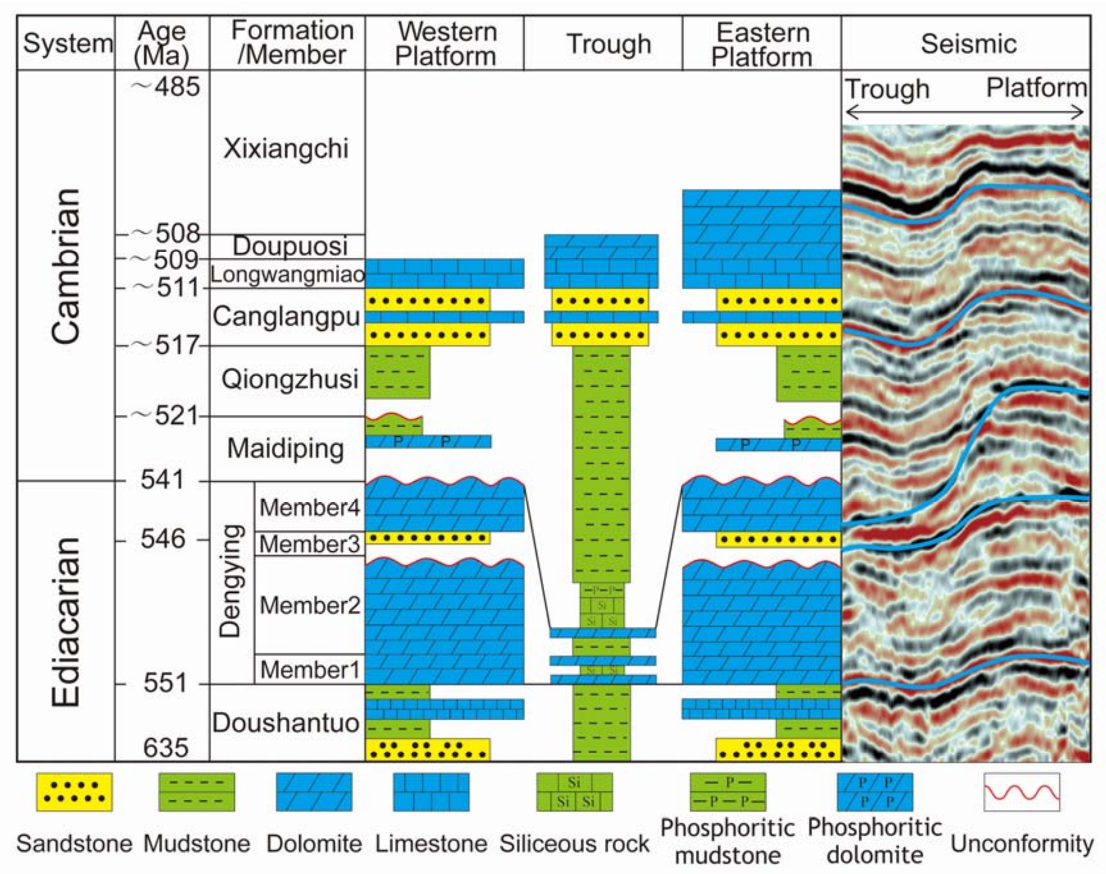

FIGURE 3 Stratigraphy of Ediacaran to Lower Cambrian rocks in the Sichuan Basin, illustrating variation in thickness and lithology across the carbonate platforms and trough. The seismic expression of the mapped stratigraphic events is shown in column on the right. The Ediacaran System (Sinian in Chinese literature) consists of the Doushantuo Formation of the Lower Ediacaran and the Dengying Formation of the Upper Ediacaran. The Dengying Formation comprises four members, Member 1 to Member 4 (Z_2dn^1-Z_2dn^4 in Chinese literature). The Lower Cambrian consists of the Maidiping, Qiongzhusi, Canglangpu, and Longwangmiao Formations. The Dengying Formation thins from the platform margins to the trough, while the Lower Cambrian thickens within the trough.

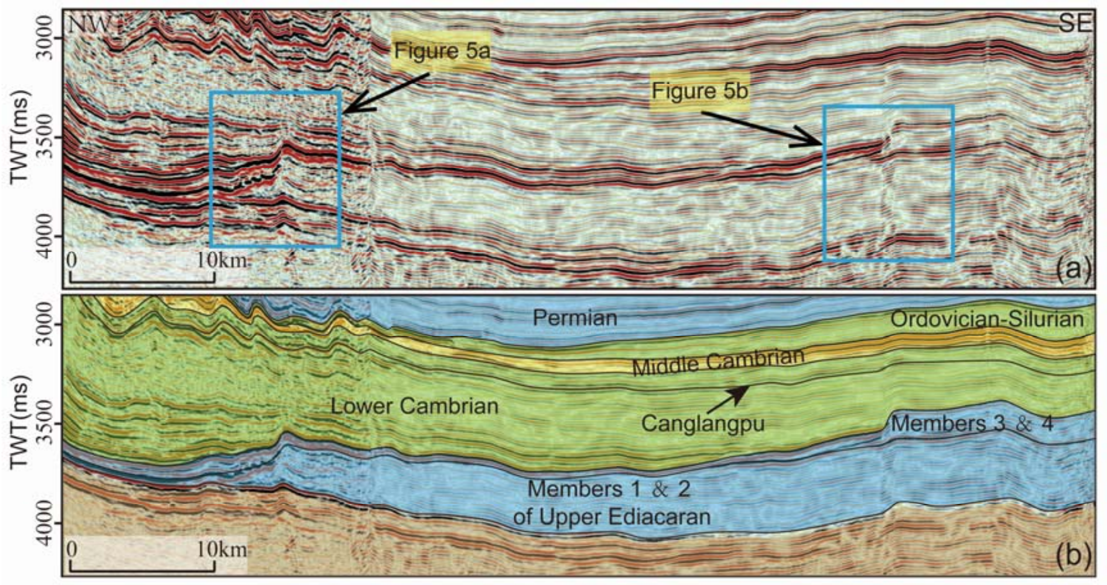

FIGURE 4 Seismic section A across the northern part of the intraplatform trough (location shown on Figure 2); uninterpreted (a) and interpreted (b). The sections show the thinning of the Dengying Formation to the NW (blue Members 1-2 of Upper Ediacaran), the development of the two platform margins, the filling of the trough and onlapping of the platform margin by the Lower Cambrian. Note the distance over which the Member 4 platform margin has back-stepped.

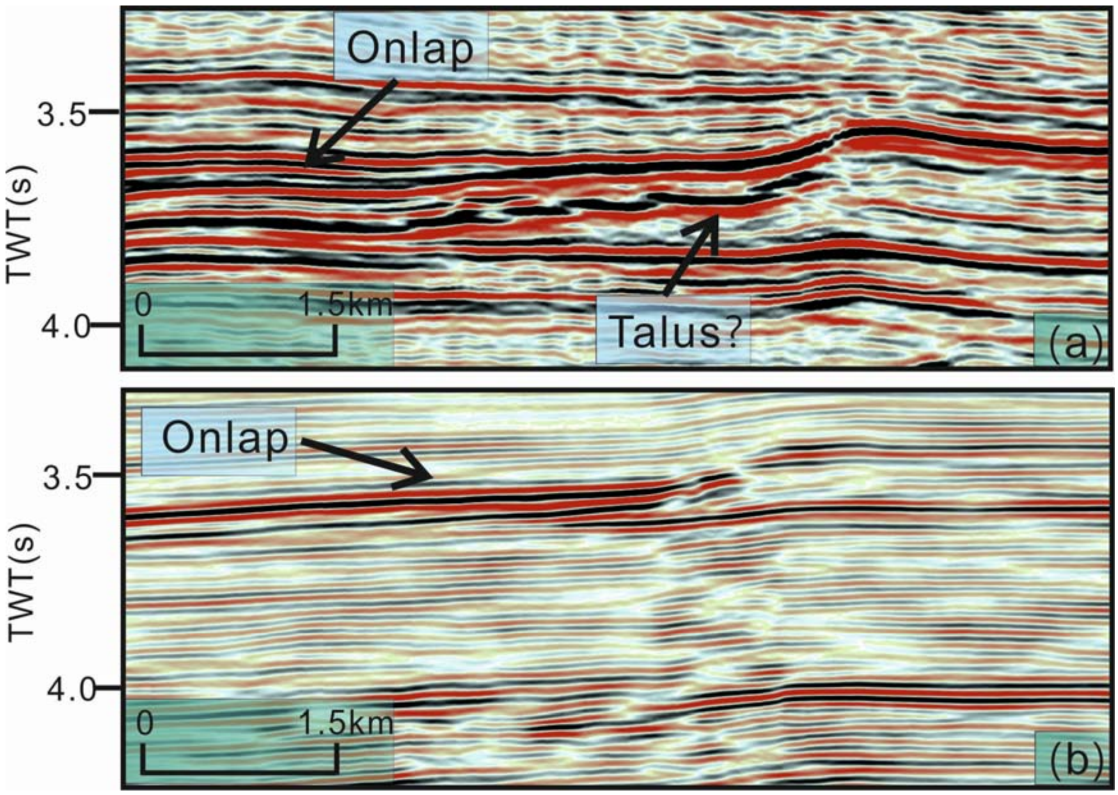

FIGURE 5 Seismic sections illustrating detail of the older (a) and younger (b) platform margins from seismic line A; location shown in Figure 4a. Data are shown at approximately a 1:1 scale. Section (a) images the first platform margin; the disrupted

reflections are interpreted as talus deposits; onlap of the Lower Cambrian is evident. Section (b) shows the second platform margin and onlap of the Lower Cambrian in more detail.

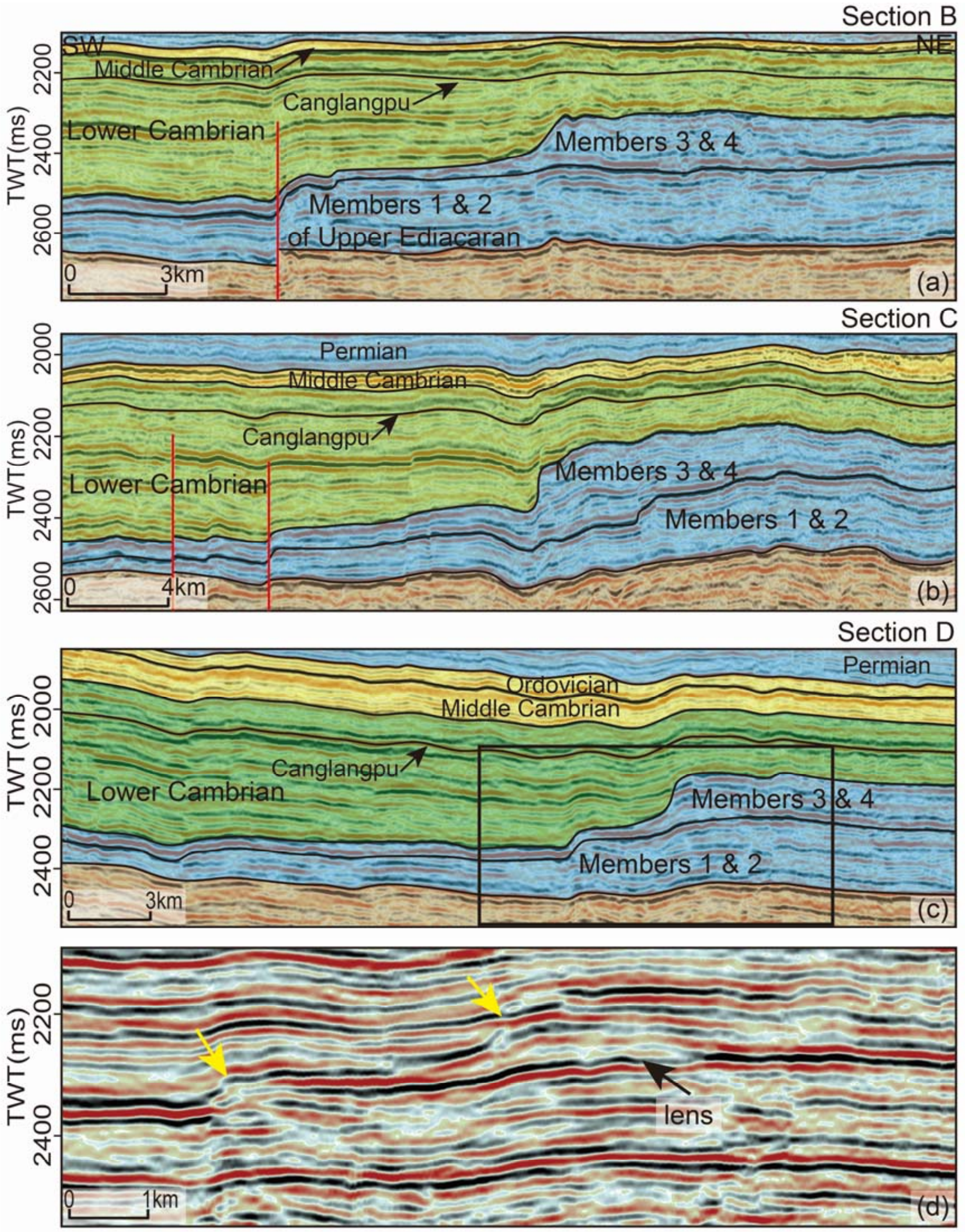

FIGURE 6 Seismic sections B, C, D, perpendicular to the trough margin in the centre of study area. Sections are located on Figure 2. All three sections image both platform margins, and onlap of the Lower Cambrian. Potential clinoforms associated with the younger platform margin are visible in Section C (arrowed). The fourth section is a detail of the youngest platform margin (arrowed). Note the lensoid body associated with the platform build-up.

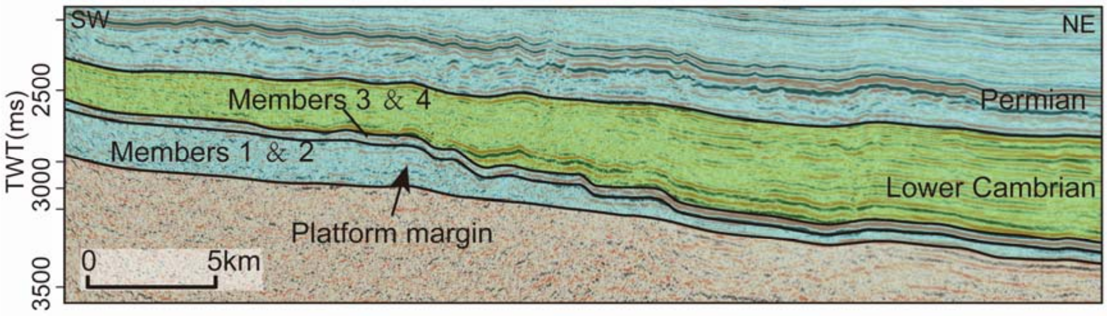

FIGURE 7 Seismic section E from a 3-D dataset located on western margin of the trough, showing the older platform margin, with Cambrian strata onlapping the relief associated with the platform edge. The seismic line is located is on Figure 2.

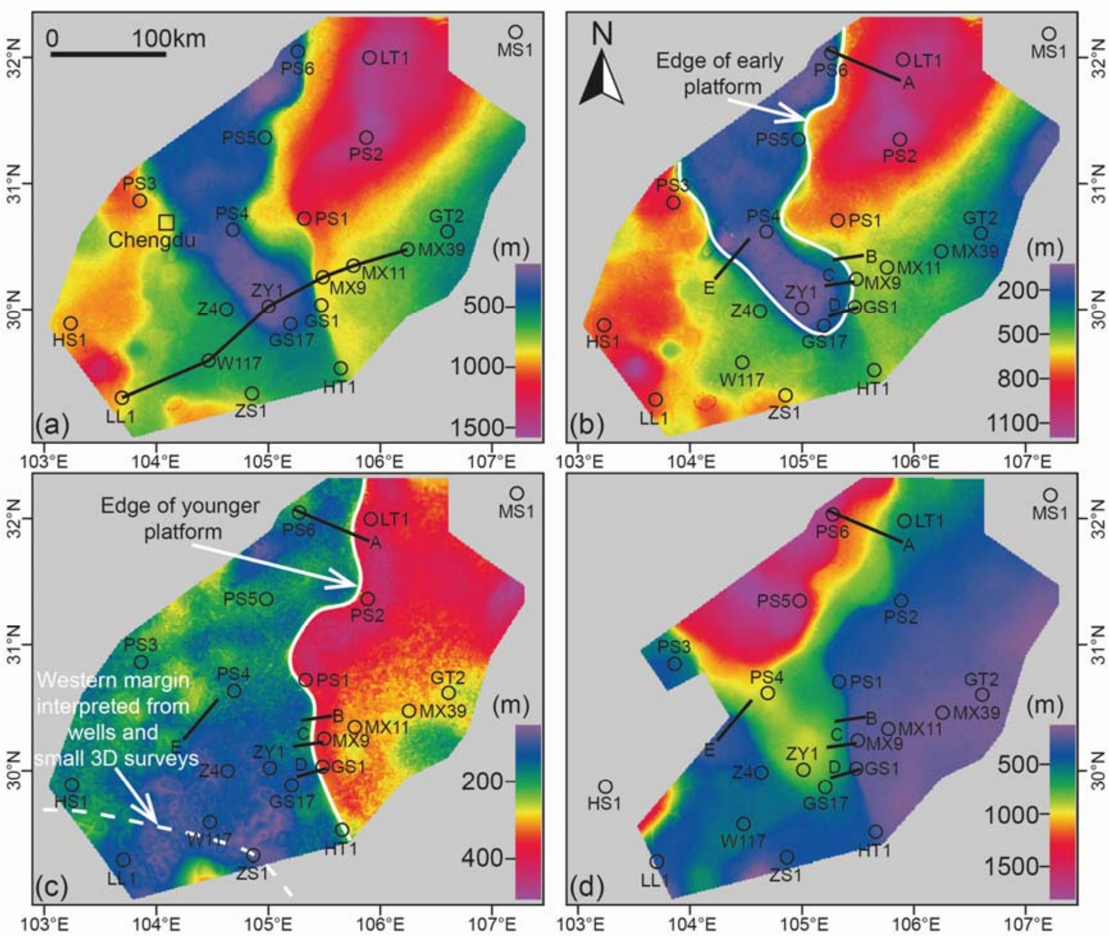

FIGURE 8 Isopach maps of the Upper Ediacaran to Lower Cambrian. (a) Isopach map of all members of the Dengying Formation which shows a NW-SE oriented low widening to the N, with thick carbonate platform margins on the E and W flanks of the trough. (b) Members 1 and 2 isopach map. The thickness change from the platform margin to the trough allows the margins of the oldest platform to be clearly located. (c) Member 4 isopach map shows the location of the younger platform margin on the E side of the trough. (d) The isopach map of the Lower Cambrian shows the main Early Cambrian depocentre as the sediments infilled the trough. Solid circles are sites of the wells used in the paper, including six pseudo wells PS1-PS6. Black line in Figure 8(a) is the location of the well correlation shown in Figure 9.

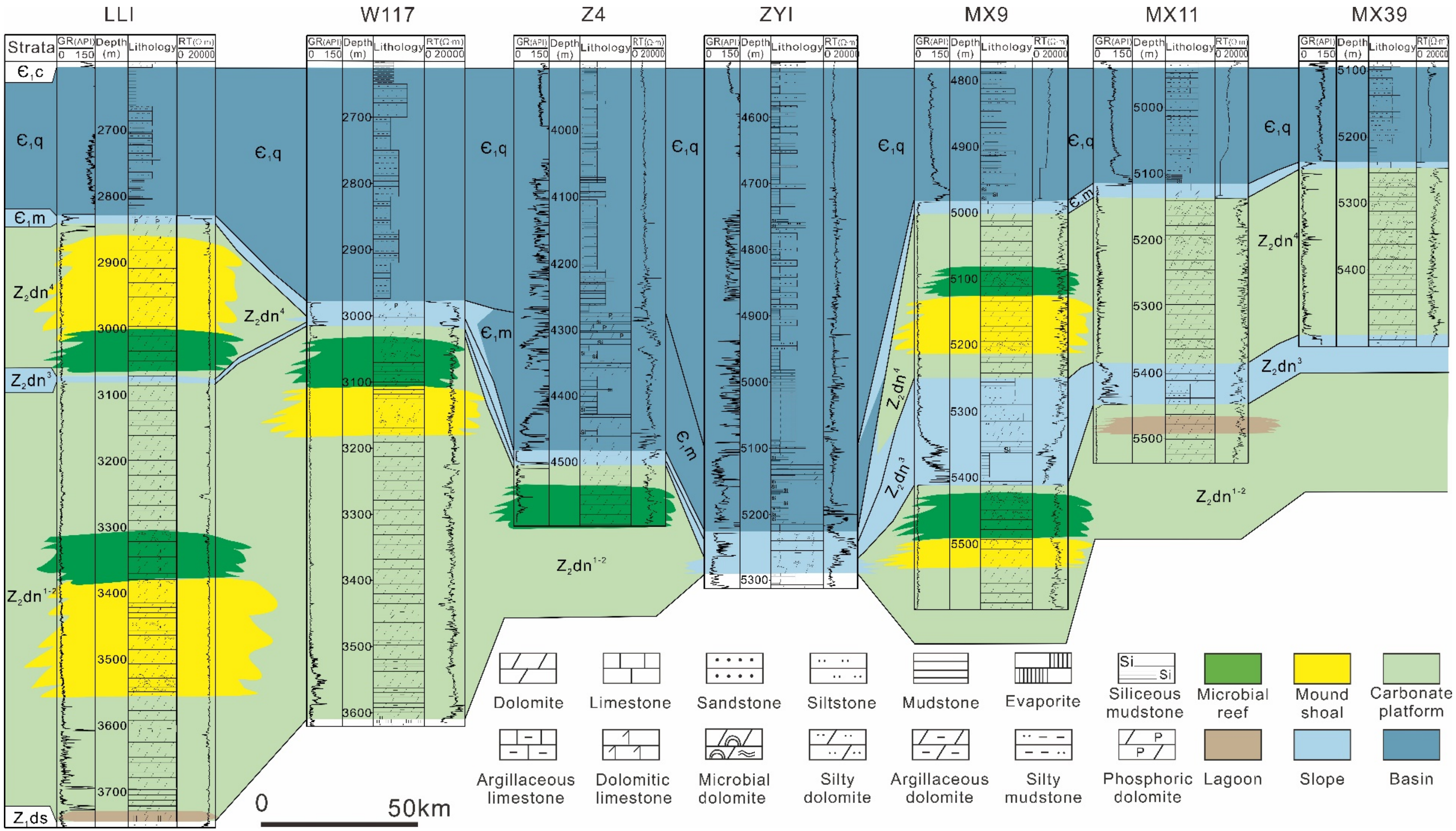

FIGURE 9 Well correlation for the Upper Ediacaran to Lower Cambrian units from SW (left) to NE (right) across the intraplatform trough (see Figure 8 for location). Note the considerable thickness variations of the Dengying Formation (Z_2dn^{1-2}, Z_2dn^4) and Lower Cambrian ($Є_1m$- $Є_1q$) across the trough and adjacent platforms.

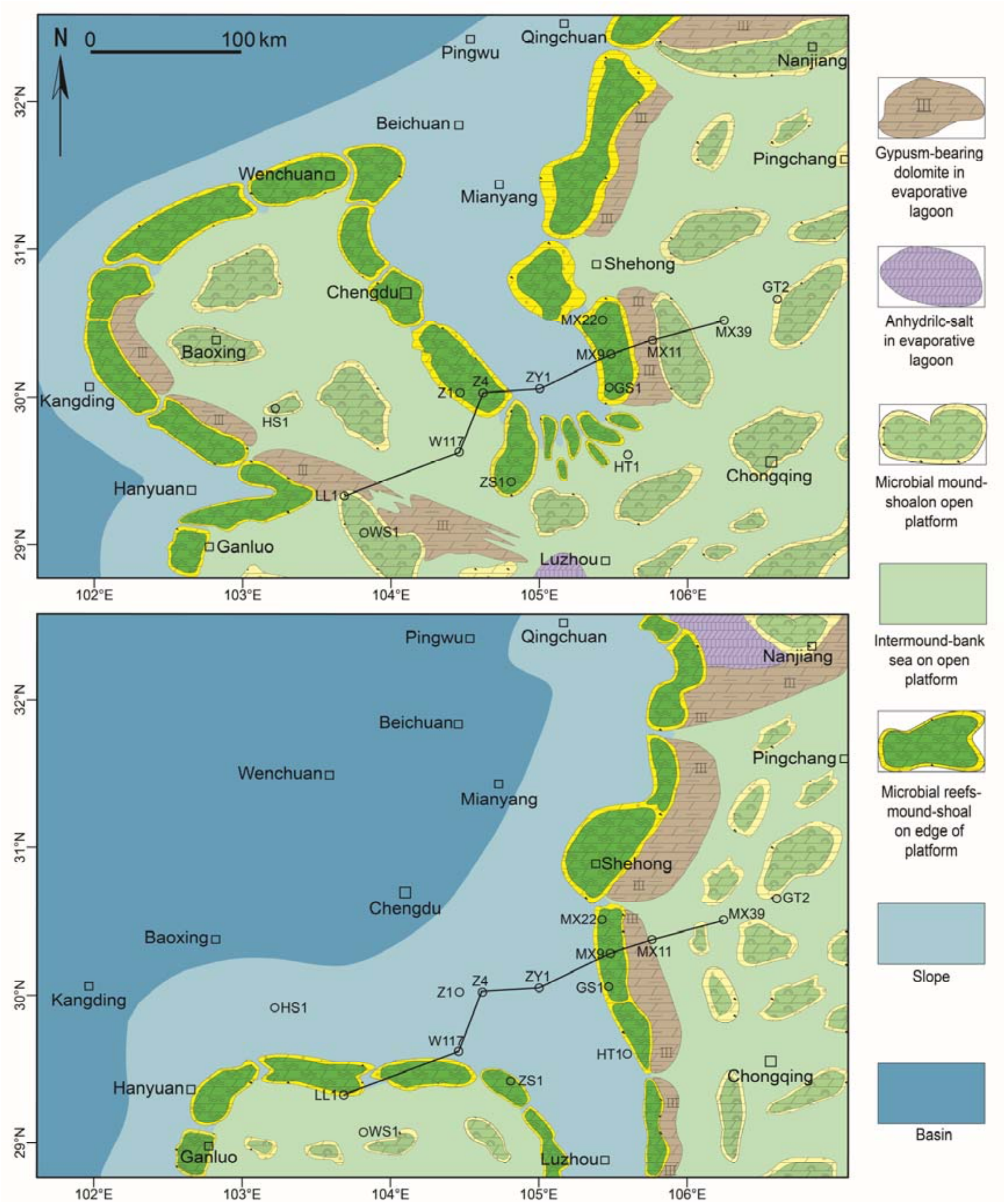

FIGURE 10 (a) Palaeogeography of Member 2 of the Dengying Formation (Z_2dn^2) based on the interpretation of seismic data, well logs and cores. Microbial mounds and shoals are abundant on the platform margins forming long narrow belts. (b) Palaeogeography of Member 4 of the Dengying Formation (Z_2dn^4) based on the interpretation of seismic data, well logs and cores. The black line is the locations of the well correlation in Figure 9.

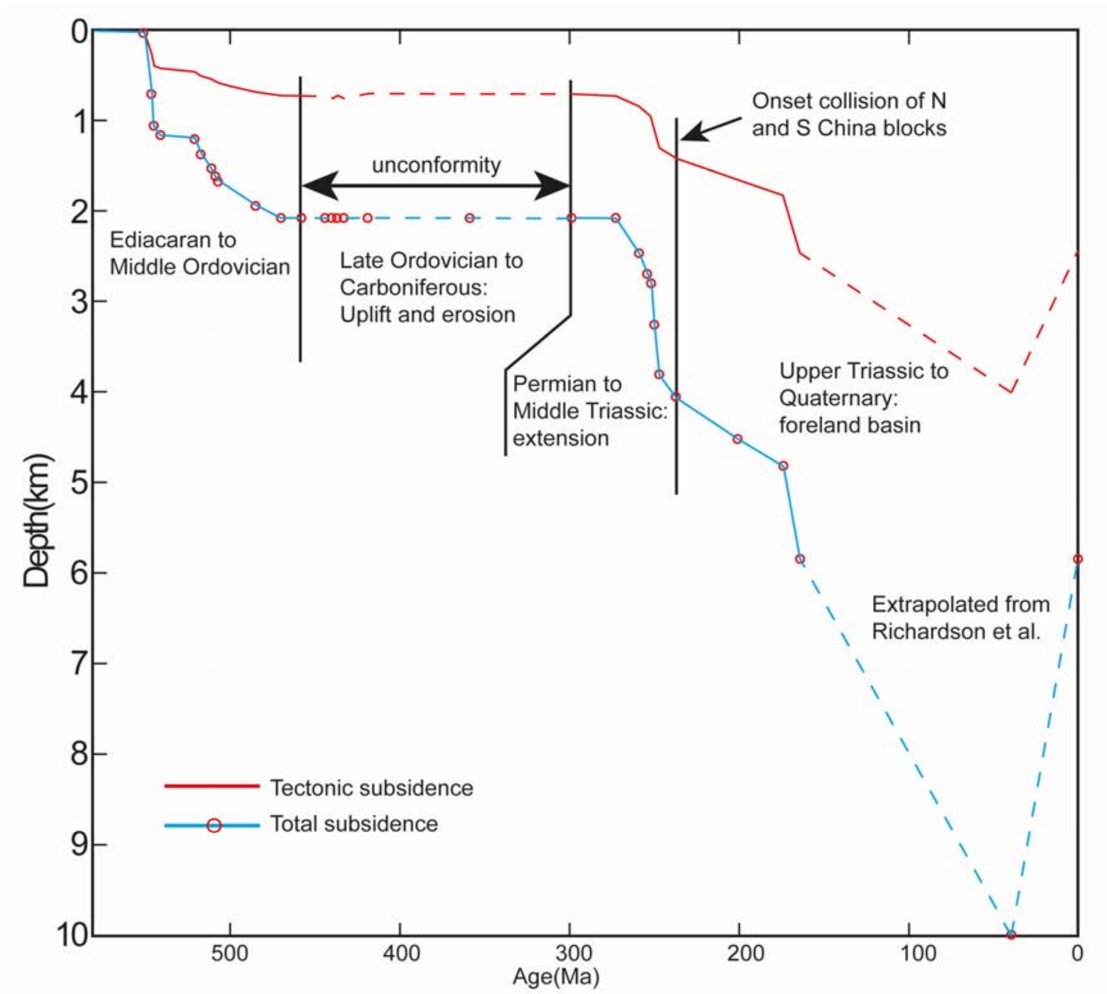

FIGURE 11 Subsidence curves of well GS1 in the centre of the basin illustrating the main basin forming events in the Sichuan Basin. Blue line is the decompacted subsidence; red line is the backstripped water-loaded subsidence. Data in Richardson et al. (2008) was used to give a semi quantitative estimate of what the maximum foreland basin subsidence might have been assuming 4 km of erosion of late Jurassic to Tertiary sediments in the last 40 Ma.

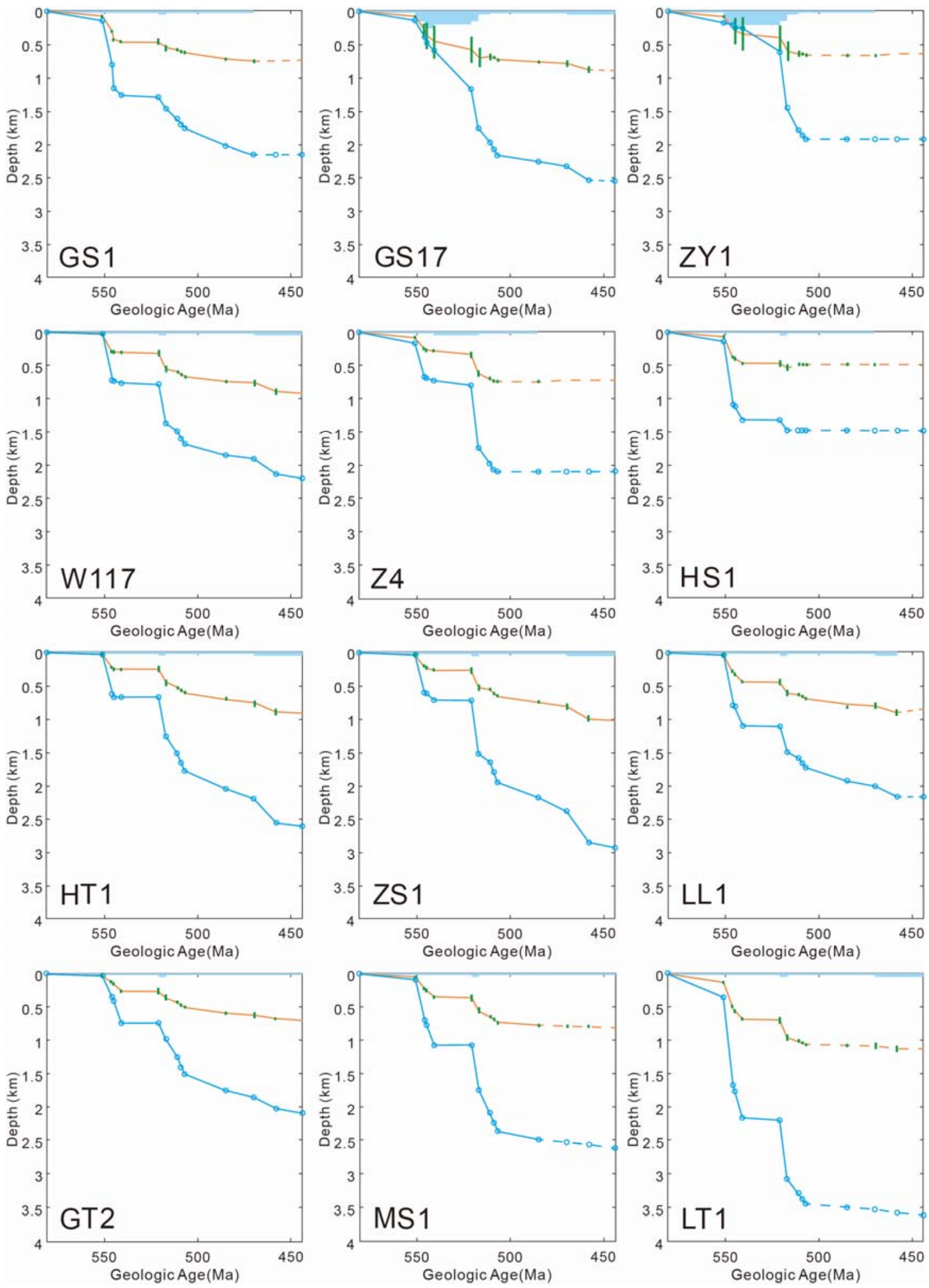
GS1
GS17
ZY1
W117
Z4
HS1
HT1
ZS1
LL1
GT2
MS1
LT1
Depth (km)
Geologic Age(Ma)
0
0.5
1
1.5
2
2.5
3
3.5
4
550
500
450

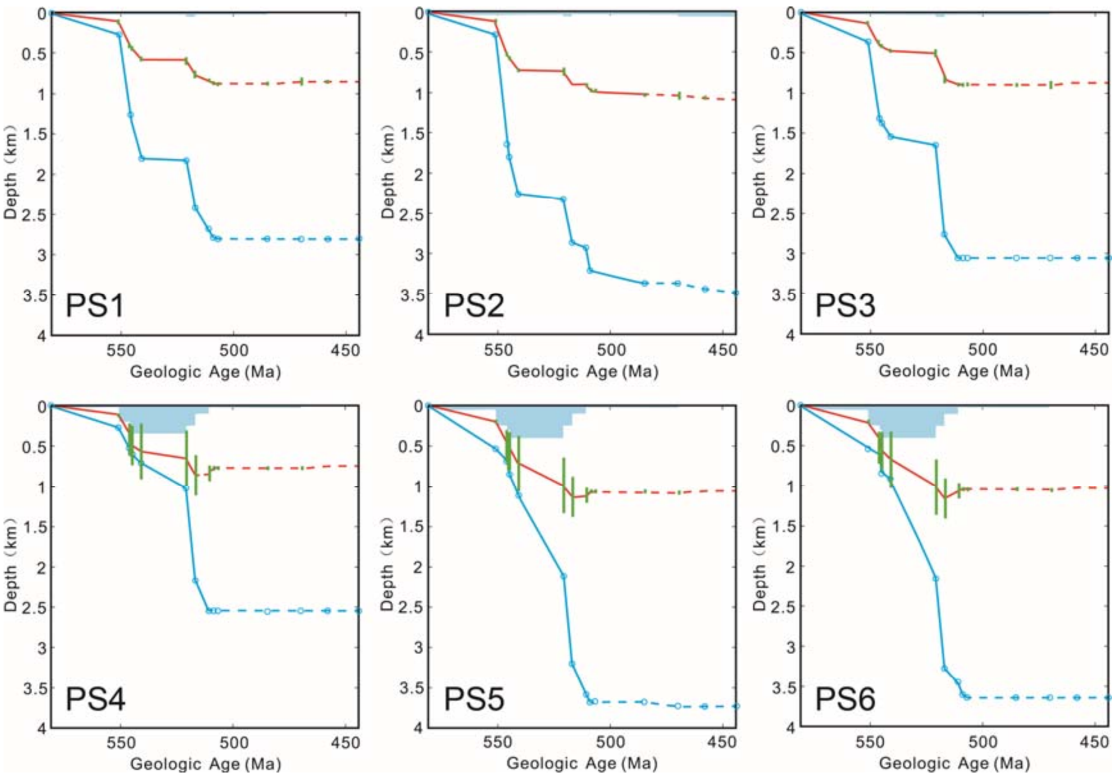

FIGURE 12 Decompacted subsidence curves (blue lines) and backstripped water-loaded tectonic subsidence curves (red lines) for 18 wells/pseudo wells in the basin; wells are located in Figure 2. The subsidence curves in many of the wells are affected by later tectonic movement during the Late Ordovician to Silurian causing considerable uplift and erosion, such as ZY1, Z4, HS1, LT1, and PS1 to PS6; missing sections are shown by dashed lines.

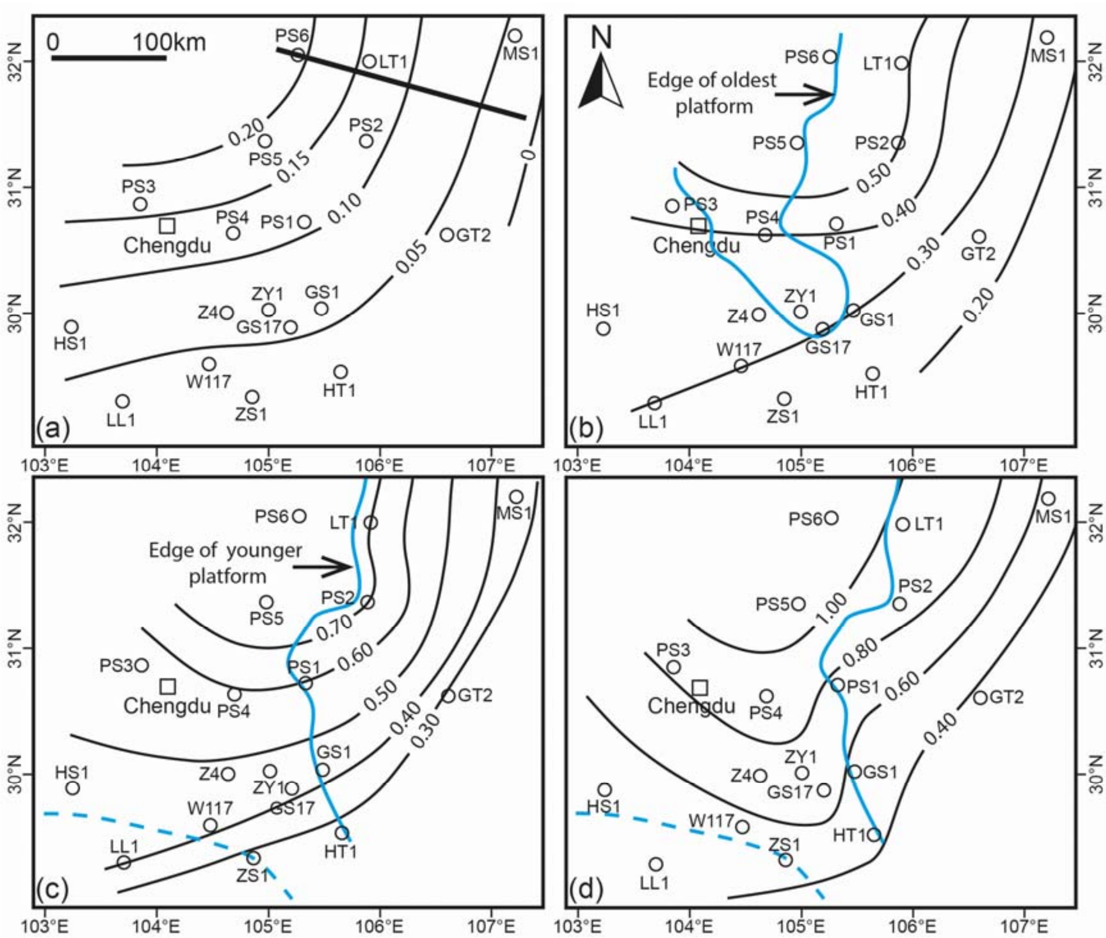

FIGURE 13 Contours of the cumulative tectonic subsidence in kilometers during the Ediacaran to Early Cambrian. (a) Early Ediacaran (equivalent to the Doushantuo Formation); (b) early Late Ediacaran (equivalent to $Z_2dn^{1\text{-}2}$); (c) late Late Ediacaran (equivalent to Z_2dn^4); (d) Early Cambrian (equivalent to the Maidiping and Qiongzhushi Formations). The platform margins (in blue) are shown for reference. Note in Early Cambrian times (d) the trough was being infilled and the carbonate platform was no longer active. The solid line is the location of the cross section in Figure 14.

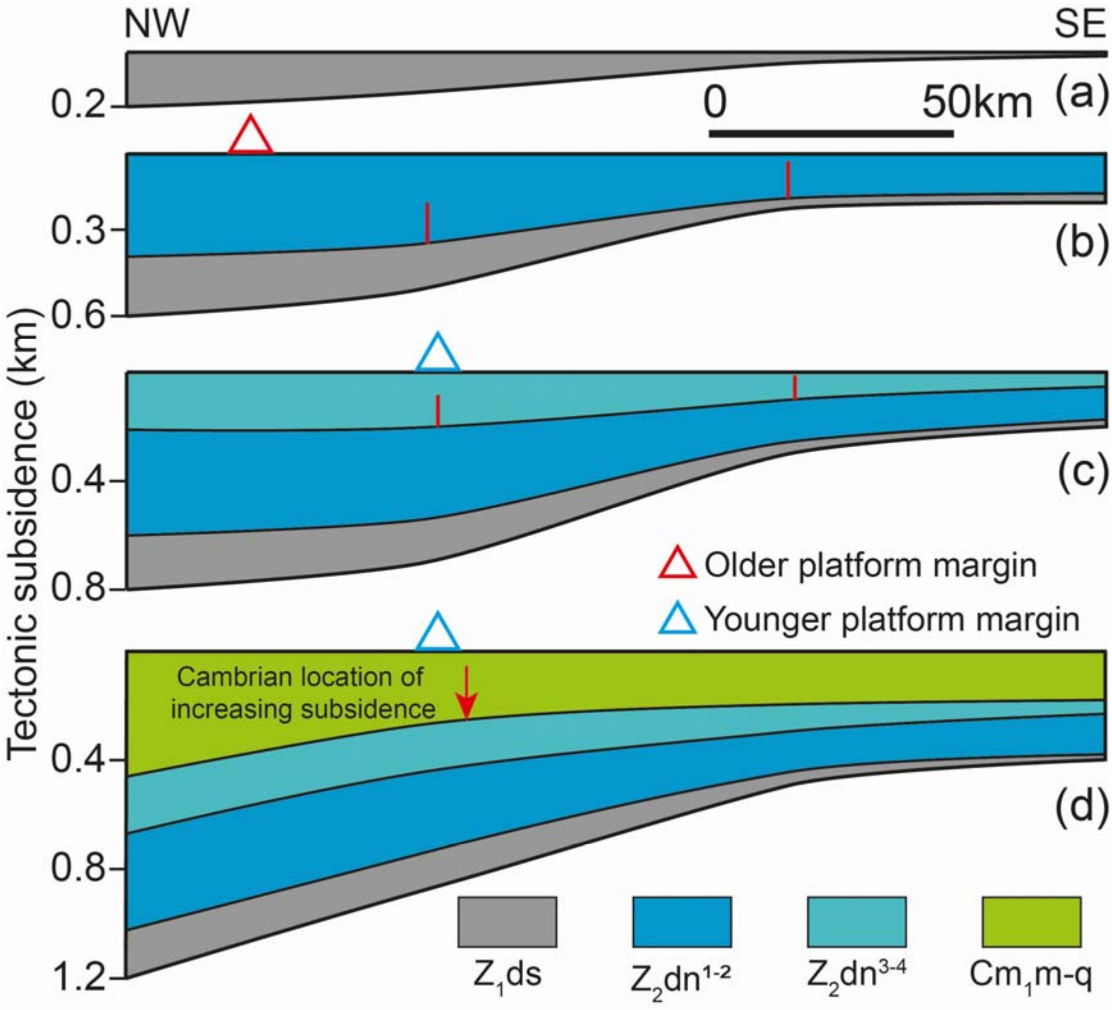

FIGURE 14 2-D reconstruction of backstripped tectonic subsidence from the Ediacaran to Early Cambrian calculated from subsidence contours. (Section located in Figure 13). Note lack of correlation between increased gradient in subsidence at Dengying Formation times (Between red lines) and location of the platform margins. (a) Early Ediacaran (equivalent to the Doushantuo Formation); (b) early Late Ediacaran (equivalent to $Z_2dn^{1\text{-}2}$); (3) late Late Ediacaran (equivalent to Z_2dn^4); (4) Early Cambrian (equivalent to the Maidiping and Qiongzhushi Formations, $Є_1m$- $Є_1q$).

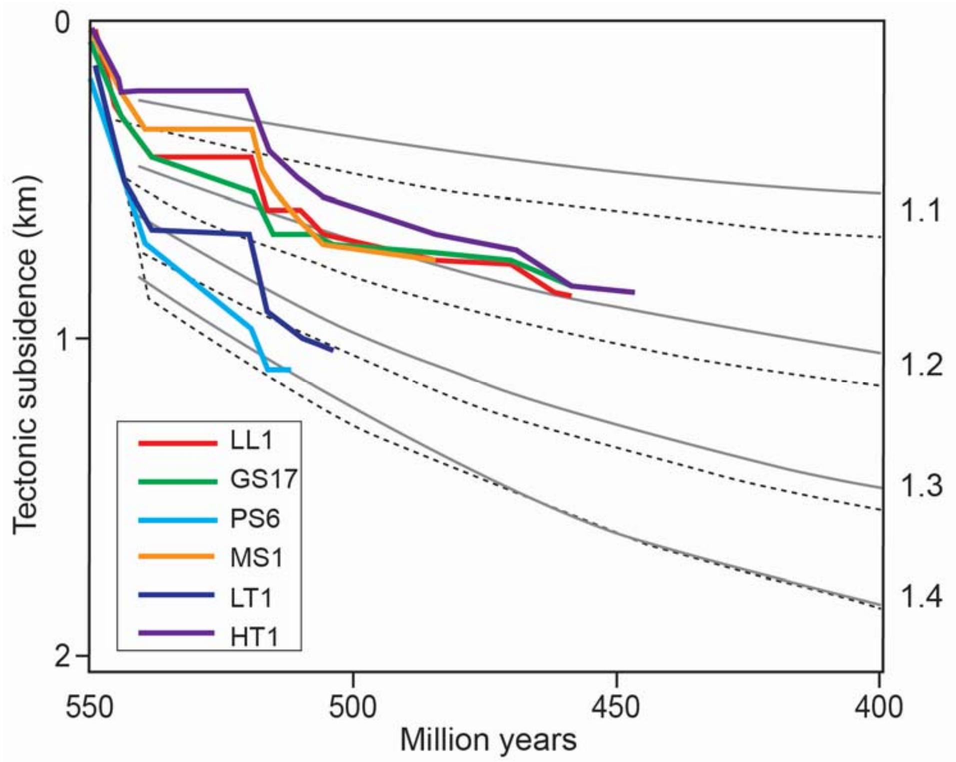

FIGURE 15 Comparison of calculated water-loaded subsidence for six locations in the Sichuan Basin (coloured lines) with theoretical models from Armitage and Allen (2010). The grey lines are for a model of instantaneous extension; dashed lines for finite extension at a slow strain rate of 10^{-15} s^{-1}. The theoretical models have a 200 km thick lithosphere, and a 40 km thick crust. The amount of lithospheric extension for instantaneous extension was low with a stretching factor of ~1.2 (wells LL1, GS17, MS1, and HT1), but increases in the NW part of the study area where it reaches 1.3-1.4 (wells LT1 and PS6).